Advanced Fire-Resistant Cementitious Material

Major Qualifying Project Report

Presented by:

Katherine Baker

Presented to:

Professor Nima Rahbar and the Worcester Polytechnic Institute Civil Engineering
Department in partial fulfillment of the requirements for the Degree of Bachelor of
Science

2018-2019

Abstract

Sprayed Fire-Resistant Materials (SFRMs) are usually a cement-based material. Since cement is an inherently brittle material, cracks which can expose the steel underneath the substrate can negatively affect the performance of the material during a fire. This study looks at creating an advanced flexible fire-resistant cementitious material by adding fibers to a fire-resistant cementitious composite to improve the flexural properties in the material, limit the extent of cracking, and improve the ductility of the material.

Acknowledgements

I would like to thank Professor Rahbar for his support during the entire process and for choosing me to complete this project.

I would also like to thank Professor Albano, Russell Lang, and Jessica Rosewitz for their help with some of the research and testing.

I would also like to thank Fabio Mazza and John DeVine Jr for the previous work they have done on the project.

Authorship

All sections of this report were written by Katherine Baker

Executive Summary

Steel construction is one of the most common forms of construction, as steel is highly ductile and a fairly low-cost material. However, one major drawback to using steel construction is the loss of load capacity that steel experiences when heated. The building and life safety codes (International Building Code, NFPA 5000, and NFPA 101) require certain elements of the building structure to be protected. One of the methods of protection recommended is to use Sprayed Fire-Resistant Materials (SFRM)s. SFRMs can be applied directly to the steel. However, there are some problems with current SFRMs. Most SFRMs are held together with cement, which is an extremely brittle material. This can lead to extensive cracking in the SFRM which can expose the steel the material is supposed to cover. This study looked at improving the mechanical properties of SFRMs.

In the proposed SFRM, there are four main materials. Cement was used as a binder. Sodium Bentonite was used to increase the workability of the mix, a fine aggregate and as a secondary binder. Garden grade vermiculite was used as a lightweight aggregate and was chosen due to its capacity to absorb water. Nylon fibers were used as a reinforcement to increase the tensile and flexural capacity of the material.

Three different test batches were tested using a four-point bend to look at the flexural behavior of the samples. The first test batch was a replication of the process used by a previous student on this SFRM. The second test batch used a modified mixing process and the third used the modified mixing process, but the samples were mechanically vibrated before curing. Once the optimal mixing process was determined, compression cylinders and Brazil Disks were cast and tested.

During the testing, the modified mixing process flexural samples were all found to have behavior similar to high-performance high-ductility fiber reinforced concrete, reached a stress of 1 MPa before the first crack occurred and withstood a strain of more than 3% before the load capacity dropped more than 20%. The compression tests and Brazil Disk tests confirmed the high ductility of the material from their cracking patterns and the failure patterns the samples produced.

Capstone Design Statement

The Accreditation Board for Engineering and Technology (ABET) requires that all accredited engineering programs include a capstone design experience. At Worcester Polytechnic Institute (WPI), this requirement is met through the Major Qualifying Project. The capstone design must address many of the following realistic constraints of a project: economic, environmental, sustainability, constructability, ethical, health and safety, social, and political. This Major Qualifying Project (MQP) focuses on designing a fire-resistant protective coating by adding fibers to improve the flexural properties and ductility of an inherently brittle cementitious material.

The economic aspect is fulfilled by the use of materials that are commonly found and used for other applications and are relatively inexpensive to purchase. The constructability aspect is fulfilled by development of a mixing process for the material that was developed in this project. The health and safety aspects are fulfilled by the intended use and reasoning behind the development of SFRMs. SFRMs are designed to give occupants of a steel structure enough time to escape before the building collapses in the case of a fire. The coating will potentially increase the safety of the building, if properly maintained.

Professional Licensure

The requirements for achieving Civil or Environmental Engineering licensure vary state-by-state. The first step in the licensure process is to obtain a degree from an ABET-accredited program. Upon graduation, a person can become classified as an Engineer-in-Training (EIT) by taking and passing the Fundamentals of Engineering (FE) exam. This test proves that the person has a thorough understanding of the basics of engineering. There are many resources available to help prospective EITs succeed with this step.

The next step is to gain professional experience, usually by working under a licensed engineer at a firm. The general timeframe for this is four years. During this time, it is important to become familiar with your state's specific requirements for licensure. A detailed application must be submitted that documents this experience.

Finally, the Principles and Practice of Engineering (PE) Exam can be taken. Again, there are many resources available to help people prepare for the PE exam to ensure success. There are several reasons why it is beneficial to obtain the title of Professional Engineer. With this distinction, future employers are aware of the skill a person possesses and the time that has been invested. Additionally, clients can be assured that the work you provide is sound and reliable. Being licensed is more than just knowing the technical aspects; by taking the PE exam, a person is committing to follow the ethical obligations of the profession, as well.

Table of Contents

Chapter 1: Introduction

Fire resistant assemblies are required by both the International Building Code (IBC) and the Life Safety Code (NFPA 101). In order to achieve the specified level of fire resistance, some materials need to be protected. Steel is an example of one such material. When heated, steel does not burn, but the load capacity rapidly drops as the temperature increases. To increase the time the steel will continue to hold the load, some material must be applied to the steel. When exposed to about 1000ºF (538ºC), a steel member will expand 9 ½" which can cause problems in the building and starts to rapidly lose its ability to carry load (Brannigan, 1982). Flashover frequently occurs in compartments at similar temperatures, about 600ºC. Flashover is when the entire room is involved in the fire and once flashover occurs, anyone in the room would most likely perish. However, the loss of strength in the steel is important for the other spaces in the building, so even if the spaces are not on fire, the building now has the possibility to collapse. As the members in the compartment on fire will most likely fail and transfer the load to other members in the building, this can overstress the surrounding members, causing those to fail as well, which will eventually lead to the collapse of the building. Steel is also a conductor, so as it heats up, it can transfer the heat easily to neighboring compartments, causing the fire to spread rapidly. By protecting the steel, you can limit the heat transfer compartment to compartment and give occupants more time to evacuate.

There are a couple of materials that can be used to protect steel. Gypsum, masonry structures, concrete, sprayed fire-resistant materials (SFRMs), mineral fiberboard, or an intumescent material (Ruddy, 2003). Gypsum board and mineral fiberboard are often used to make fire-resistant barriers. Although gypsum board and mineral fiberboard assemblies are easy to install around members or to create walls, but when exposed to a hose stream, they often disintegrate even though they can survive the standardized test to determine the fire resistance of the assembly. Intumescent materials are materials that expand when exposed to heat. They are often used to seal off penetrations in a fire-resistant barrier during a fire. Firestop systems often contain a layer of intumescent material so that if the cables melt away, the barrier will still be intact. Concrete and Cementitious SFRMs use cement, which is a gypsum-based material, to insulate the steel. In concrete buildings, steel is a frequent reinforcement as concrete has little tensile strength. In cementitious SFRMs, vermiculite or pearlite is often added to the mix as a lightweight aggregate because both materials expand and insulate when exposed to heat (Ruddy, 2003). This study focuses on cementitious SFRMs which is reinforced with nylon fibers.

Chapter 2: Background

There are often problems with current SFRMs. Brittleness in the material can lead to severe cracking and often leads to large chunks falling off the structure. Figure 2.1 shows an example of the damage that can occur from the cyclic loading structures face.
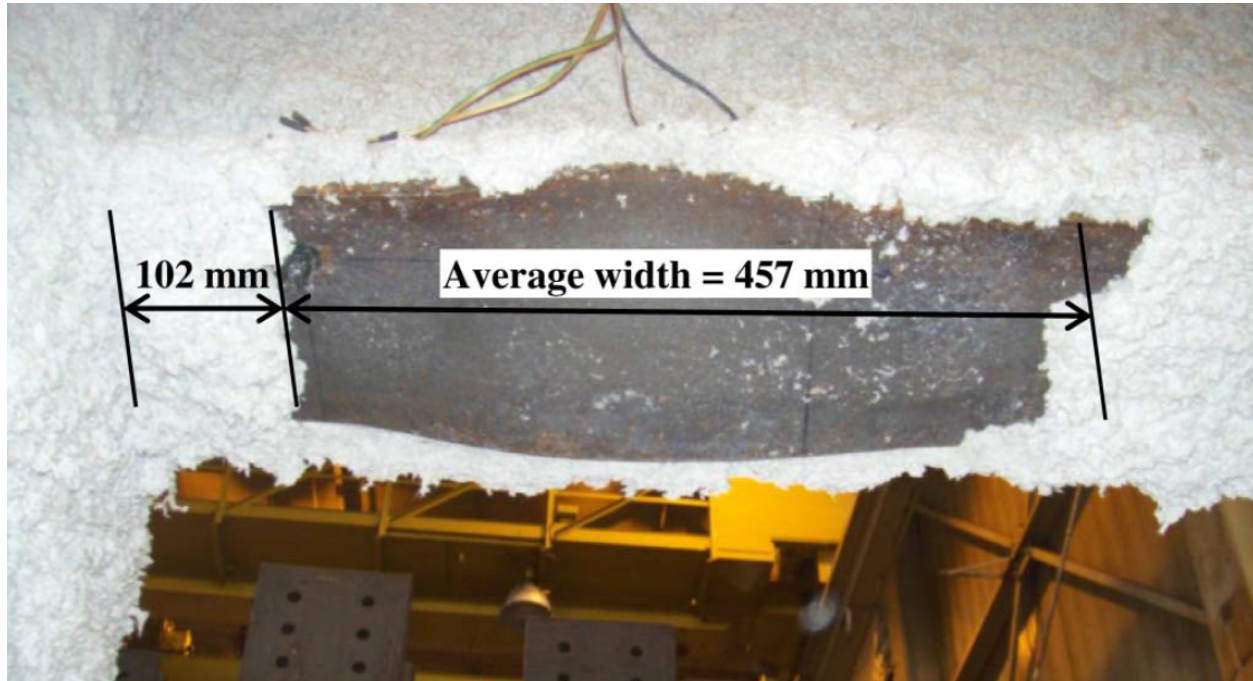

Figure 2.1: Example of SFRM damage on underside of bottom flange of structure subject to cyclic loading (Braxton & Pessaki, 2011)

Once this damage occurs, the steel is exposed. During a fire this exposed point, which since steel is an excellent conductor, can cause heating of the rest of the beam or column which will heat up the rest of the structure due to the interconnected members that make up the structure. Since steel's load capacity drops when heated, the steel members can buckle due to the deadweight of the building, even though it was designed to support those loads.

As concrete is a very brittle material, tensile reinforcement is often needed. Usually, steel or rebar is used in a framework like structure to reinforce the concrete. However, recently fibers have been introduced as a new reinforcement method. One class of fiber reinforced concretes (FRCs) is high performance-high ductility FRCs. This type of FRC can experience strain hardening, due to multiple cracking, where the strength continues to increase, as shown in Figure 2.2. Figure 2.3 shows the stress-strain curves for high performance-high ductility FRCs, regular FRCs, and regular concrete with no reinforcement.
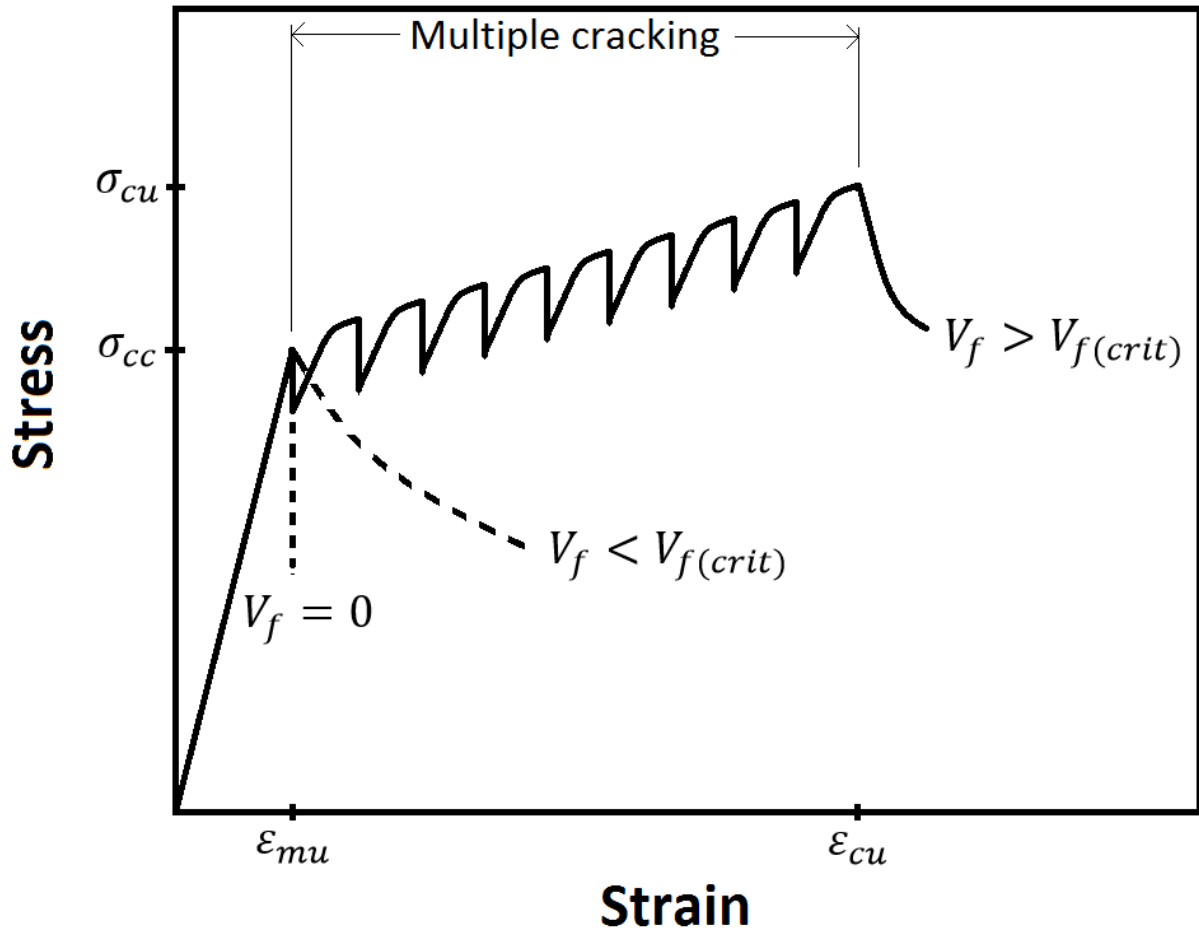
Figure 2.2: increasing strength as multiple cracks occur (Bentur & Mindess, 2007)
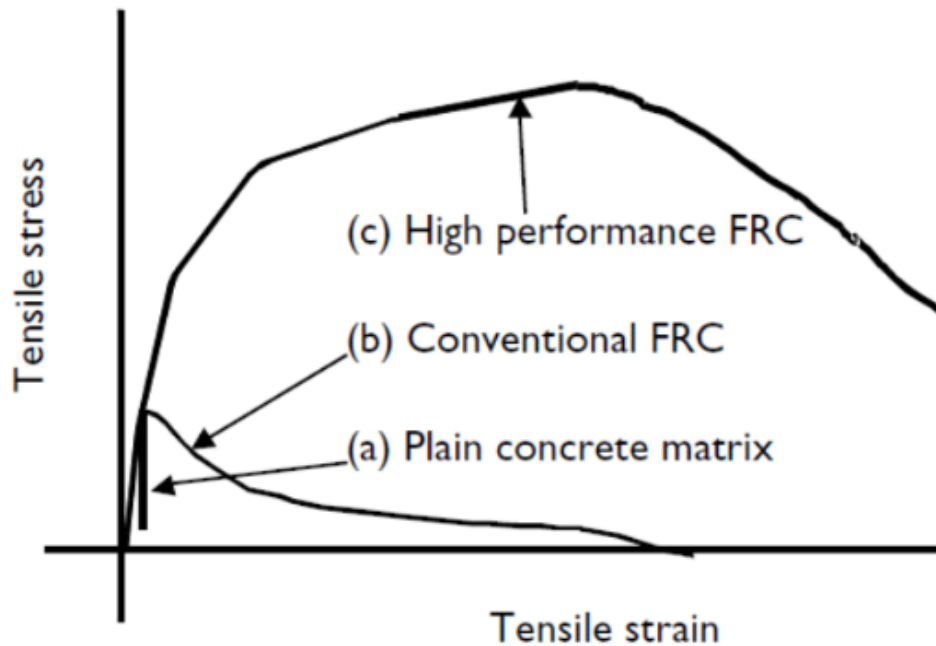
Figure 2.3: Difference in Stress-Strain curve for FRCs (Bentur & Mindess, 2007)

By adding fibers to a cementitious SFRM, this project looks to see if there will be an increase in the flexural behavior of the SFRM to try to prevent the large gaps that can occur from the extensive cracking in a brittle material.

Chapter 3: Materials

This chapter discusses the materials and material properties used in the SFRM.

3.1 Type I/II Portland Cement

The main material used in the SFRM was Type I/II Portland Cement. Portland Cement is the main binder in concrete. Limestone and clay materials are the main materials used to make cement (Aïtcin, 2016). Portland Cement is made up of tricalcium silicate SiO_2 - $3CaO$, dicalcium silicate SiO_2 - $2CaO$, tricalcium aluminate Al_2O_3 - $3CaO$, and ferroaluminate $4CaO$ - Al_2O_3 - Fe_2O_3. The molecules that make up the cement hydrate at different rates. There are 5 phases to the hydration process. Figure 3.1 shows a graphical representation of the heat release over time during the hydration of the cement.
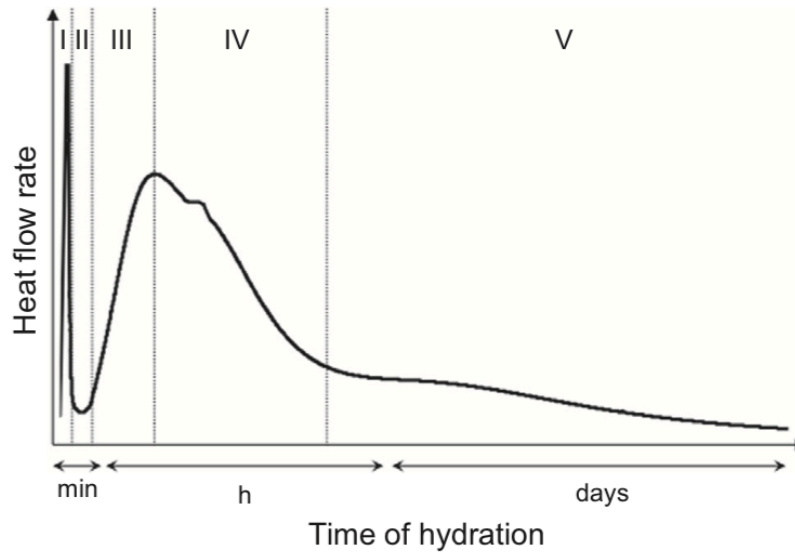
Figure 3.1: Heat release over time for hydration of Portland Cement (Aïtcin, 2016).

During Stage 1, the tricalcium silicate and tricalcium aluminate ionize and is the initial hydration stage for those molecules. Stage 2 is a dormant period. In Stages 3 and 4, the hydration of the tricalcium silicate and tricalcium aluminate continues. The hydration of the tricalcium silicate and tricalcium aluminate forms portlandite and C-S-H. C-S-H is an amorphous paste. During Stage 5, the dicalcium silicate and ferroaluminate hydrate (Aïtcin, 2016).

3.2 Sodium Bentonite

The most common use for sodium bentonite is to use it as a pond sealant or as a drilling mud. Sodium Bentonite is a good pond sealant, as the material tends to swell when exposed to water and form a low permeability layer (Papp, 1996). Companies that sell sodium bentonite have two methods they recommend for sealing a crack with sodium bentonite: either have a pure layer of sodium bentonite or mix with soil. Bentonite clays are also used to aid with cleaning out drilling holes. Drilling mud is used to bring the sediment at the bottom of the drilled holes to the surface and to help stabilize the walls of the drilled hole/shaft. Sodium Bentonite is used as a drilling mud due to the material's ability to form a low permeability layer and the viscosity of the sodium bentonite water mixture (Papp, 1996 and Grolms, 2015). Bentonite clays like sodium bentonite have been used in cementitious applications in the past as a low cost pozzolan to

partially replace ordinary Portland cement. By partially replacing the cement in the mix, this can help minimize the amount of cement that remains unreacted in the mix.

Table 3.1 – Chemical Composition of Sodium Bentonite	
Chemical Compound	**% (by weight)**
SiO_2	66.05 – 71.86
Al_2O_3	20.32 – 26.03
Fe_2O_3	2.95 – 4.65
MgO	2.35 – 3.66
CaO	< 0.23

Sodium bentonite was used as a fine aggregate in the mix design. Sodium bentonite provides insulation properties, adds workability to the mix, and aids in the dispersion of fibers throughout the mix. Table 3.1 shows the chemical composition of the Wyoming Sodium Bentonite that was used in the mix.

3.3 Nylon Fibers

Cement by itself does not have high tensile strength, so when a concrete beam fails, most of the time that is due to shear or tensile failure. Adding reinforcement can increase the tensile and flexural strength of the mix. Table 3.2 shows the properties of the nylon fibers that were used in the SFRM mix.

Table 3.2 – Nylon Fiber Characteristics	
Length – L_f (mm)	12.7
Diameter – D_f (μm)	12
Tensile Strength – σ_f (MPa)	660-1080 [13]
Strain to Failure – ε (%)	15-30 [13]
Elastic Modulus – E (GPa)	3.0-5.4 [13]

Some common fiber reinforcement is polypropylene, glass, steel or nylon fibers. Nylon fibers are used in a wide range of applications due to their strength, toughness, abrasion resistance, and fatigue resistance. During a previous investigation by Shalchy, F., and Rahbar, N., the functional group in the polymer macromolecules (HTPP and PVA) was shown to affect the adhesion energy

by changing the C/S ratio of the C-S-H at the interface and by absorbing positive ions in the C-S-H structure. These studies showed that the adhesion energy of nylon is greater than that of PVA and HTPP. The excellent material characteristics and adhesion energy of Nylon make it an ideal fiber to be used in the proposed SFRM.

3.4 Vermiculite

In order to reduce the density of the mix, lightweight aggregates should be used in the mix design. In this case, vermiculite was used as a lightweight aggregate. Vermiculite is a common material that can be found in any gardening or hardware store and is used in gardening to help condition the soil. Since vermiculite absorbs water readily, this allows the concrete mixture to have a secondary hydration reaction. Having a second hydration period allows more of the cement to react with the water, creating a more cohesive mix. In addition to vermiculite's ability to absorb a lot of water, vermiculite has a low thermal conductivity (about 0.06 W/m-K). Since vermiculite has a tendency to hold onto water, during a fire event, this can reduce the contraction effects of temperature on the specimen, and while the SFRM hardens, the water the vermiculite holds helps reduce the shrinkage that can occur. Since vermiculite pellets can be a range of sizes, Figure 3.2 shows the distribution of the vermiculite particle size.
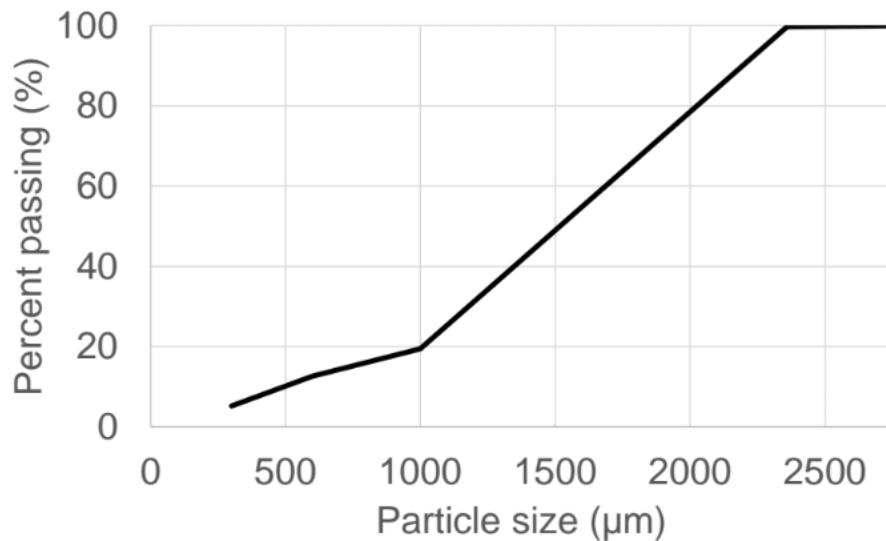

Figure 3.2: Distribution of Particle Size of Vermiculite

Chapter 4: Previous Results

This chapter discusses the previous results in Prof. Rahbar's group on this SFRM. The first section discusses the flexural properties of the material. The second section covers the thermal properties. The third section covers my process and suggestions from following the mix process provided by a previous student working on the material.

4.1 Flexural Properties

Table 4.1 shows the mix designs that a previous student tested. As the paper was incomplete, some of the language was unclear on what the ratios he used were related to. For both my results and a second student, the ratio was assumed to be related to the pounds of cement, so if 1 pound of cement was used, 1.89 lbs of water, 0.14 lbs of vermiculite, and 0.18 lbs of sodium bentonite need to be used. The fibers need to be added by calculating the volume of the mix then multiplying that by whatever the percent of fibers you need to add is.

Table 4.1 – Concrete Mix Design				
Mix design	**W/C**	**Fiber (% by volume)**	**Vermiculite**	**Sodium Bentonite**
Mix 1	1.89	1.1	0.14	0.18
Mix 2	1.89	1.7	0.14	0.18
Mix 3	1.89	2.2	0.14	0.18

In Figure 4.1, the stress strain results for Mix 1 are shown. In Figure 4.2, the stress strain results for Mix 2 are shown. Figure 4.3 shows the stress strain results for Mix 3. Figure 4.4 shows the averages for each mix on one graph. Comparing each mix, Mix 2 had the best stress-strain results, so when I decided on my mix design, I used the ratios for Mix 2 to try to replicate the results. For the methods, results, and discussion of the replication process, please refer to Section 4.3. In Figure 4.5, the cracking pattern the samples exhibited is shown.
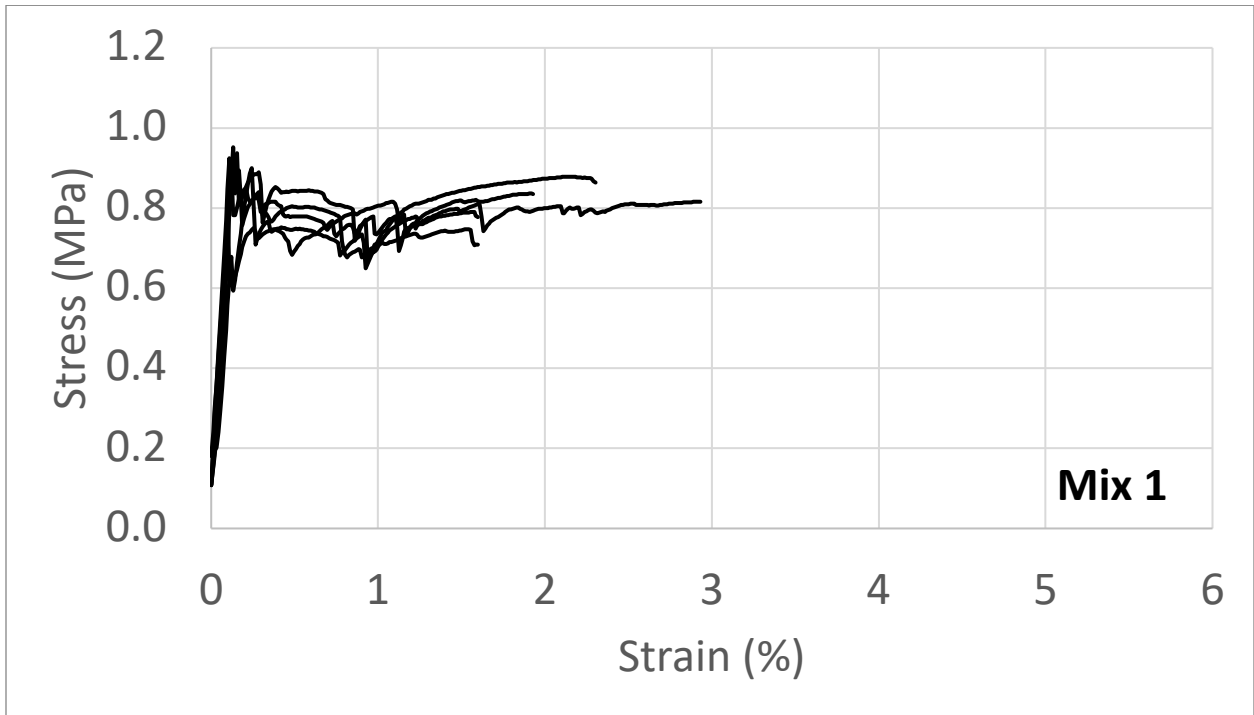
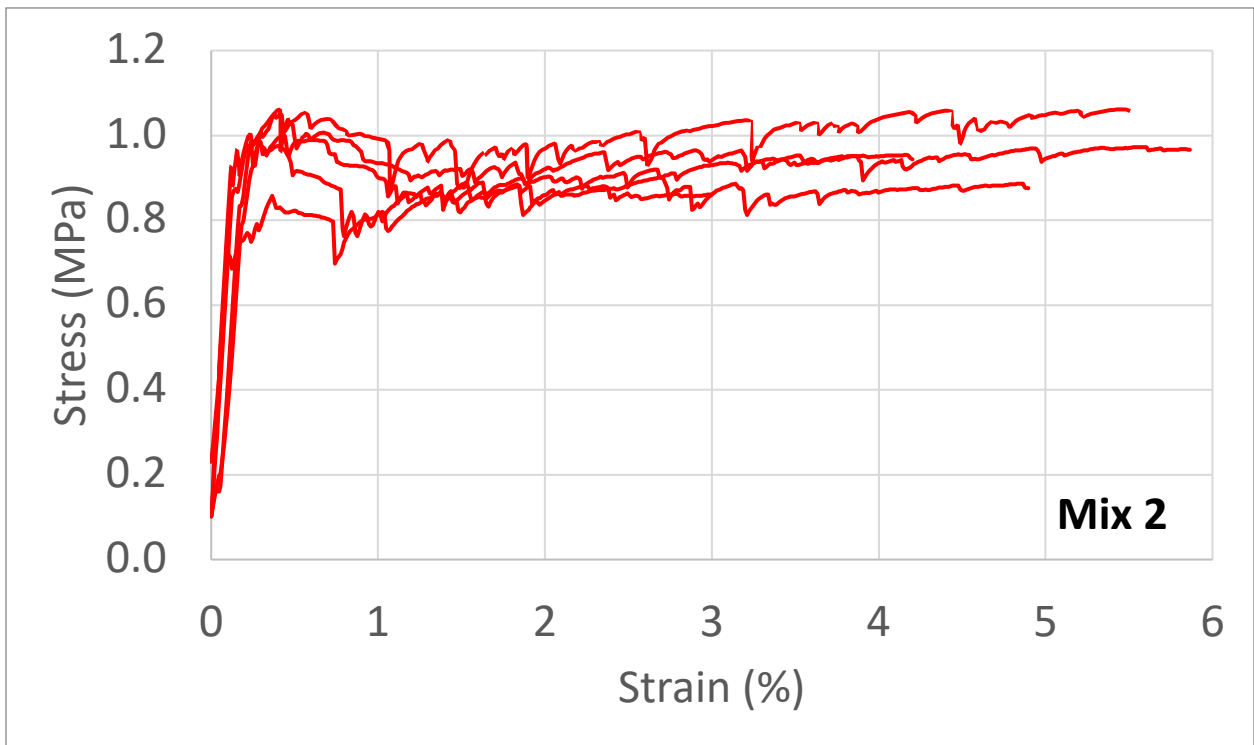Figure 4.1: Stress-Strain Results of Mix 1

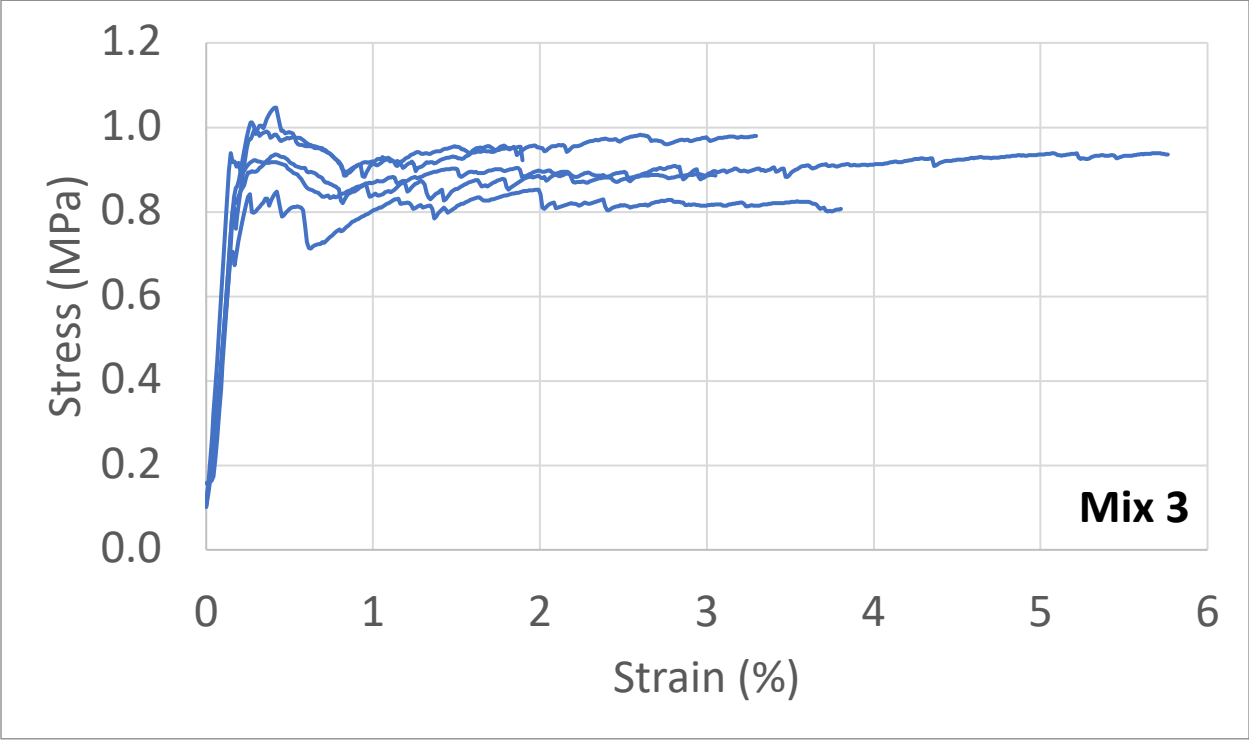Figure 4.2: Stress-Strain Results of Mix 2

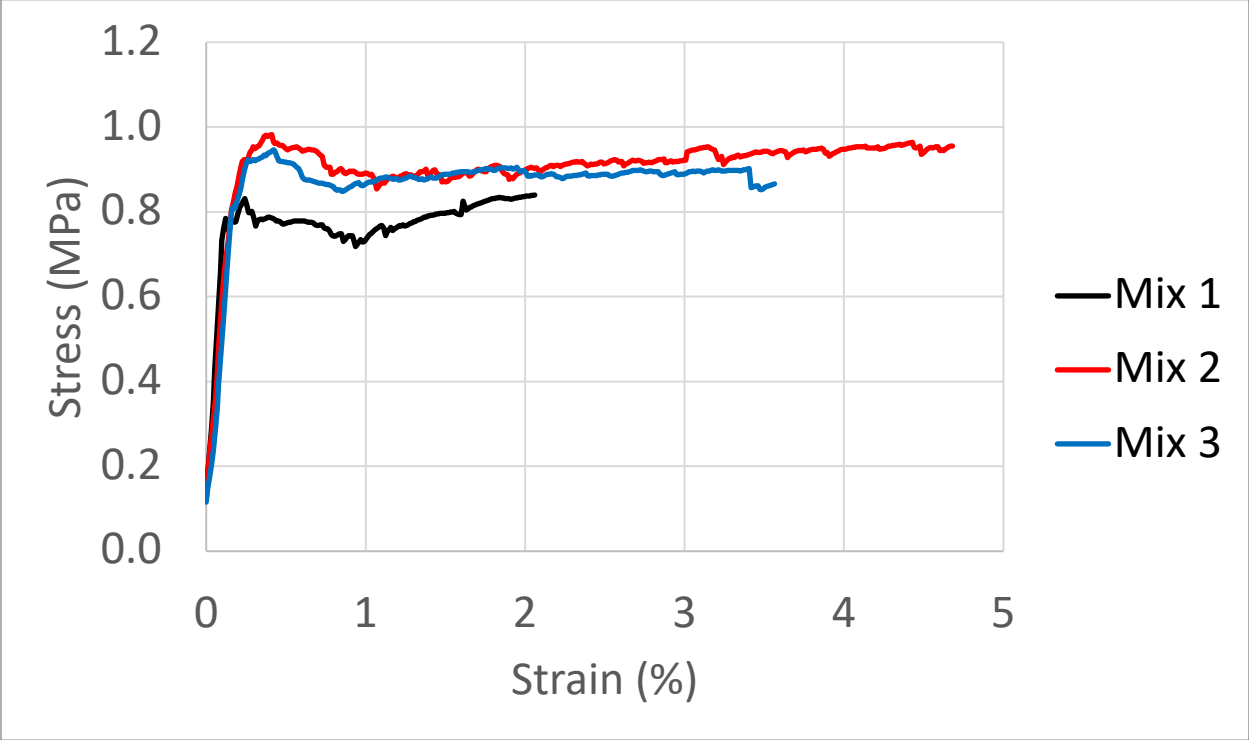Figure 4.3: Stress-Strain Results for Mix 3

Figure 4.4: Average Mix Performance

Figure 4.5: Cracking Pattern

4.2 Thermal Properties

Figure 4.6 shows the results of this testing. The graph shows the results of his mixes compared to other SFRMs. The value λ, shown on the y-axis is the thermal conductivity of the material at a certain temperature. If you look at the solid black lines, the material has a thermal conductivity of less than 0.4 W/m-K in a range of fire temperatures. At around 300°C, the thermal conductivity appears to go to 0. This occurs because at this point, the water absorbs the heat to evaporate which will cause a 0 thermal conductivity reading even though the surface temperature continues to rise.
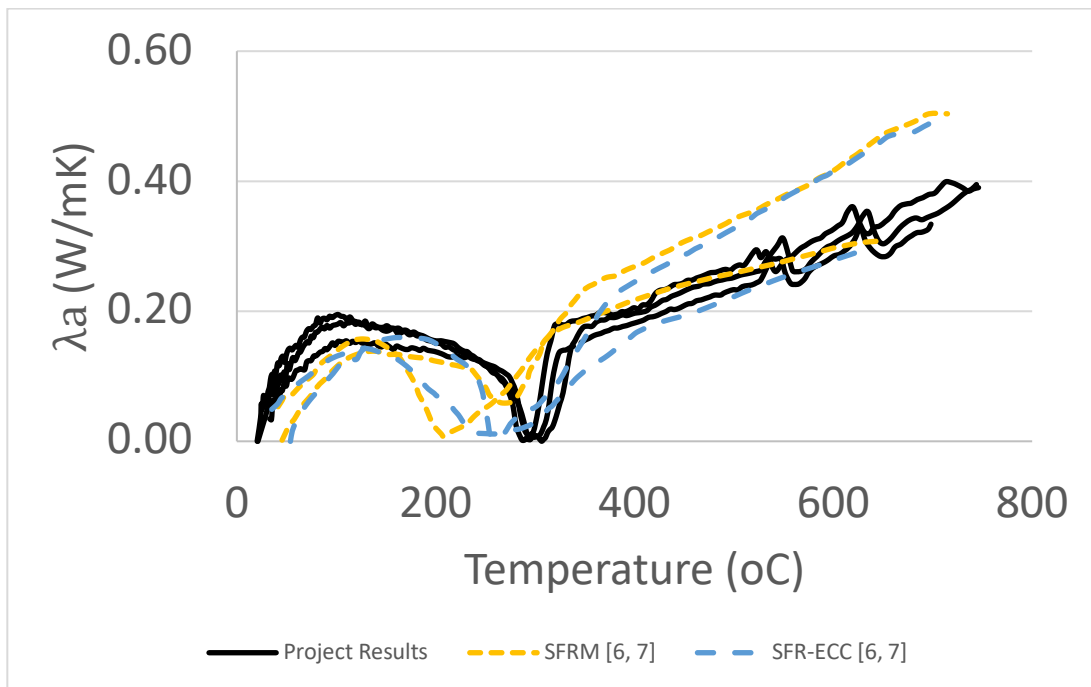

Figure 4.6: Conductivity Comparisons

4.3 Current Results

In this section, I discuss the results of replicating the previous students' work. My observations of the mixing process and the testing process are provided. I followed the mixing process provided by a previous student.

4.3.1: Mix Design and Process

The mix design I used was as seen in Table 4.2. This is the second mix from a previous student.

Table 4.2: Amount of materials			
Nylon Fibers [volume percentage]	Water [mass of water/mass of cement]	Sodium Bentonite [mass of SB/mass of cement]	Vermiculite [mass of vermiculite/mass of cement]
1.7%	1.89	0.18	0.14

The sodium bentonite was soaked in 10% of its mass of water and the vermiculite was soaked in 325% of its mass in water. These amounts were included in the water/cement ratio. The volume of fibers to be added was calculated by calculating the volume of the mix, then multiplying that number by the percentage specified in Table 4.2, which was then converted into mass to get the mass of fibers to be added.

4.3.1.1: Mixing Observations

During the mixing process, a couple of observations were noticed. The previous students presoaked the sodium bentonite in 10% of its mass in water for 24 hours prior to mixing, but during that process for me, the sodium bentonite just clumped and when I mixed it into the rest of the ingredients, the clumps made it so that the sodium bentonite might not have been evenly distributed throughout the mix. Since sodium bentonite is a pozzolan, which can be used as a cementitious material substitute, I would recommend not presoaking it in water, but rather mixing it into the cement first before the water and presoaked vermiculite is added, since the purpose of the sodium bentonite is to replace some of the Portland Cement. The process should be similar to making a cake, the dry ingredients are mixed together so that the particles are evenly distributed throughout the mix before the wet ingredients are added, which in this case are the vermiculite and water, so that when the wet ingredients are added, they can evenly react with the dry ingredients.

Another observation involves the actual method of mixing itself. The mixer used was similar to a regular kitchen stand mixer, with a paddle attachment, so in order to completely mix all the ingredients in evenly, I would recommend adding the water into the bowl first, then the cement and sodium bentonite mixture, then the vermiculite, and then fold the fibers into the mix. If the water were added in first, then the dry ingredients would combine better, and would result in more consistent data.

A third observation was regarding the process of putting the mix into the molds. When I put the mix into the molds, the fibers made it difficult to smooth the exposed surface of the wooden molds. As a result, during the testing, I used the smaller side as my testing surface. One possible improvement to the molding process could be to use a vibrator to aid with getting a smoother top rather than just using a straight edge to manually smooth the top.

4.3.2: Testing the Samples

4.3.2.1: Testing Observations

In my first mix, I tested 8 samples at 14 days. The samples underwent a load of 1.4 mm/min using a 4-point bend setup, as shown in Figure 4.7. Since the exposed surface from the molding process was quite rough, I tested the samples with the shorter edges (37 mm) as the top and bottom surfaces of the specimen and the longer edge (65 mm) as the depth of the specimen. I used a loading span of 120 mm, and a total span of 240 mm.

Figure 4.7: The Testing Setup

During the testing, the cracks that formed usually extended about 2/3 to 3/4 of the depth of the specimen. The specimens never fully broke, since the fibers held the cracks together.

Figure 4.8 shows one of the cracks developed in Specimen 2. Similar cracks formed in every sample tested. Due to these crack propagations, I was able to observe that the fibers were evenly distributed throughout and did not settle to the bottom of the sample during curing.

Figure 4.8: A crack formed in Specimen 2

4.3.2.2: Testing Results:

The beginning section of the stress-strain curve from my tested samples is fairly similar to a previous student's samples, but instead of staying relatively constant, eventually my stress values started to gradually drop as the strain increased. The value of the stress started to decrease for most samples at around a strain of 2% (see Figure 4.9), while Fabio's remained relatively constant until about 6% (see Figure 4.2).
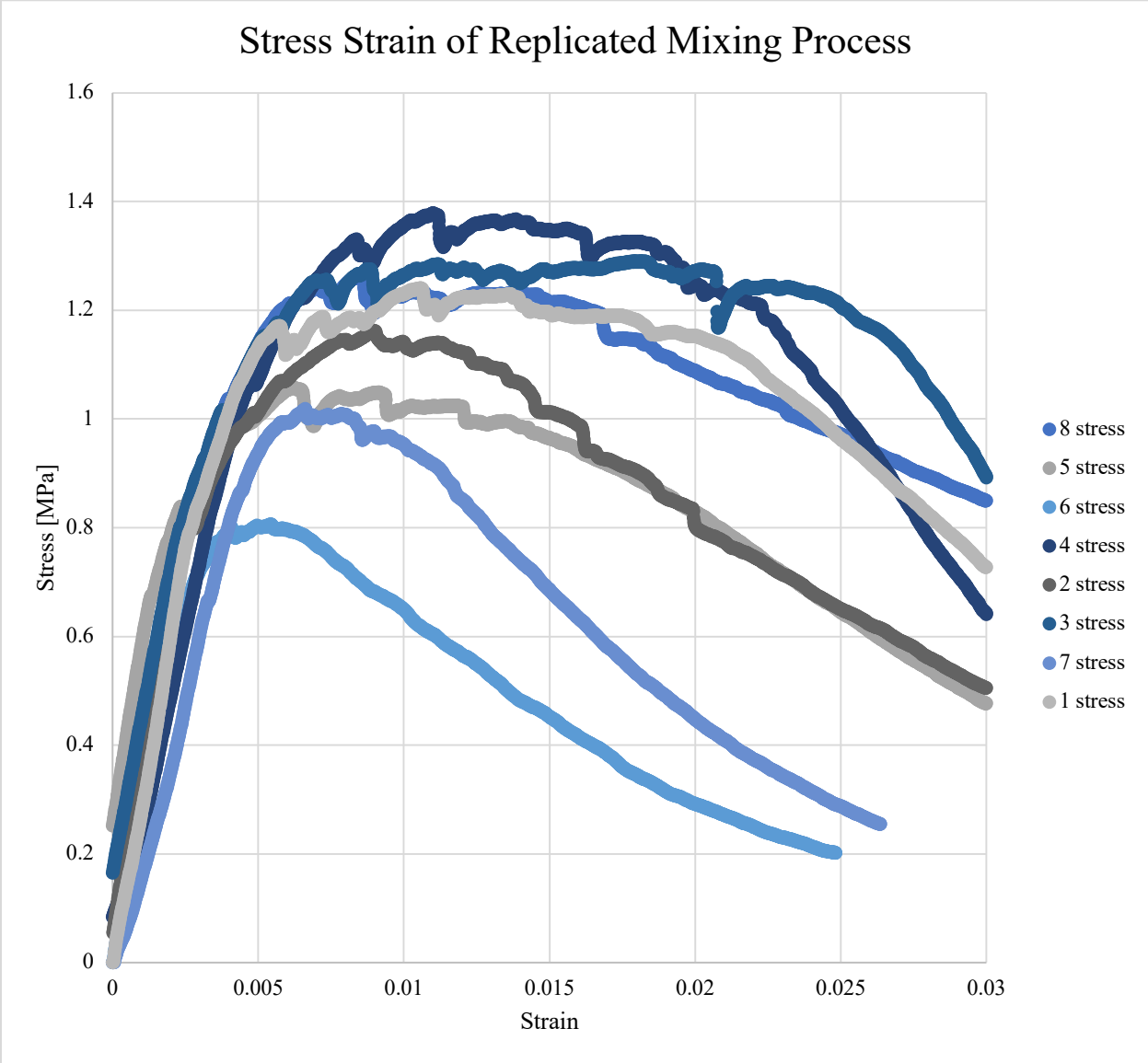
Figure 4.9: Stress-Strain Curve of All 8 Specimens Tested

Chapter 5: Methods

This chapter discusses the methods used in this study. The mix design and mixing process are discussed. The flexural testing procedure, compressive strength procedure, Brazil disk procedure and associated calculations are detailed below.

5.1 Mixing

5.1.1 Mix Design

I used the second mix design of the first student and the first mix design of the second student for my testing (see Chapter 4 for Previous Results). Table 5.1 shows the proportions that were used.

Table 5.1: Amount of materials			
Nylon Fibers [volume percentage]	Water [mass of water/mass of cement]	Sodium Bentonite [mass of SB/mass of cement]	Vermiculite [mass of vermiculite/mass of cement]
1.7%	1.89	0.18	0.14

The vermiculite was soaked in 325% of its mass in water. These amounts of water were included in the water/cement ratio. The volume of fibers to be added was calculated by calculating the volume of the mix, then multiplying that number by the percentage specified in Table 5.1, which was then converted into mass to get the mass of fibers to be added.

5.1.2 Mixing Process

There were a couple of different methods of mixing that I used. The first method I used, I followed the steps laid out by a previous student. Since this gave varied results during the testing, I altered the process slightly. Instead of presoaking both the sodium bentonite and the vermiculite, I presoaked only the vermiculite (see section 4.3.1.1 for observations and rationality behind the decision).

The first step I performed was measuring out and presoaking the vermiculite. 24 hours later, the vermiculite was about three times the original volume and I measured out the rest of the materials: Type I/II Portland Cement, sodium bentonite, the remaining water and the fibers.

One important thing to keep in mind is the order the ingredients are added to the mixer. Since the mixer used was similar to a kitchen standmixer, the order the materials are added matters. For this type of mixer, add the water into the bowl first, this will help the materials mix

evenly. Then add the cement and sodium bentonite, the vermiculite should not be added directly into the water, since it will absorb almost all the water. Next add the vermiculite and start to mix the ingredients on a lower speed. Once the materials look combined, turn up the mixer and mix for about 3-5 minutes, the mix should look and sound slightly watery. Then turn off the mixer and add the fibers. Mix slowly for about 1-2 minutes. Then remove the bowl from the mixer and mix by hand for about 15 cycles, this will help if any of the fibers are stuck to the side of the bowl. Then put the material into the 1.5" X 2.5" X 10" molds, mixing by hand for 10-15 cycles in between filling each mold. For the third test batch of the mix, I used the modified mixing process described above and vibrated the samples.

5.2 Flexural Testing

5.1.1 Testing Procedure

For this study, I tested my specimens using a four-point bend. The specimens I tested were 1.5 in by 2.5 in by 10 in. Due to the rough surface on the 65 mm (2.5 in) sides, I used the smaller edge, 37 mm (1.5 inches), as the top and bottom surfaces of the sample. The samples underwent a load of 1.4 mm/min using a 4-point bend setup, as shown in Figure 5.1. I tested the samples with the shorter edges (37 mm) as the top and bottom surfaces of the specimen and the longer edge (65 mm) as the depth of the specimen. I used a loading span of 120 mm, and a total span of 240 mm.

Figure 5.1: Testing Setup

I calculated the applied moment, the second moment of area, the engineering stress and the engineering strain. In a 4-point bend test, the middle of the span, where the loading span is, there is no shear through that section, which results in the loading section being in pure bending. In the figure below (Figure 5.2), a diagram of the theoretical loading pattern is shown.
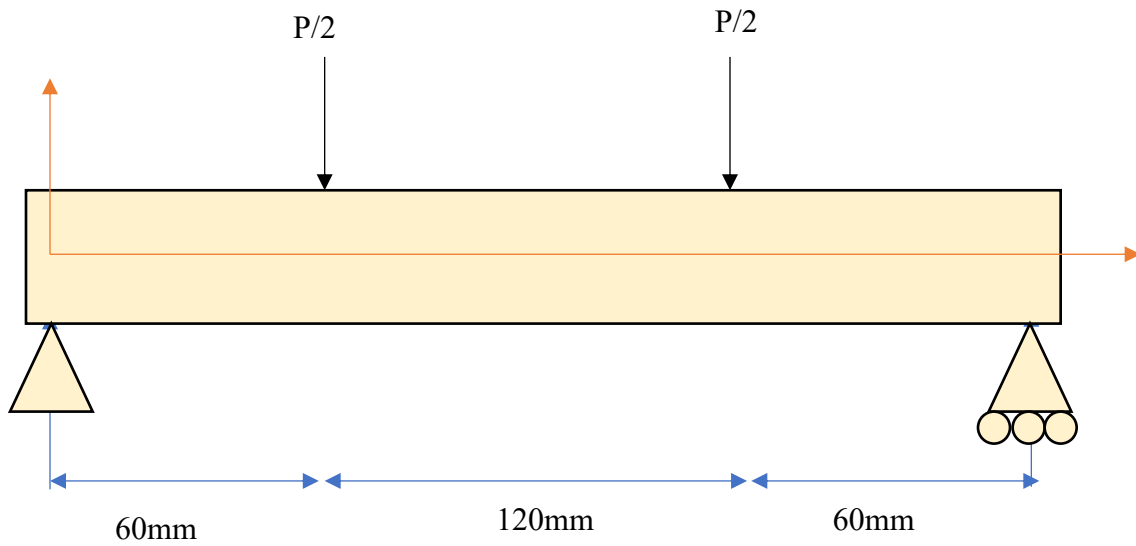
P/2   P/2

60mm   120mm   60mm

Figure 5.2: Theoretical Loading of the Specimen

First, I solved for the support reactions. In this case, both reactions are going to be +P/2. Then I systematically made cuts through the beam to develop shear and moment diagrams. Figure 5.3 shows the shear diagram on the top and the moment diagram on the bottom.
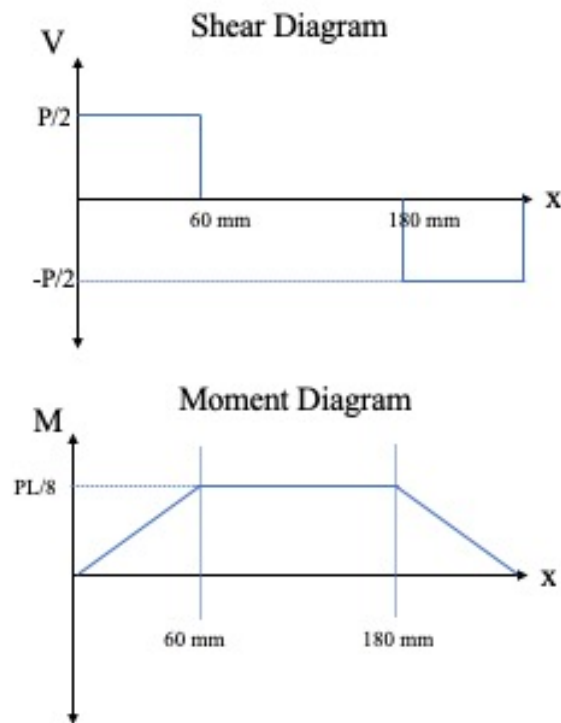

Figure 5.3: Shear and Moment Diagrams for 4-Point Bend Test

Since the loading span is where the maximum moment occurs, this is the value, PL/8, I used for my calculations, where P is the applied load and L is the total span, 240 mm. To calculate the second moment of area, I_z, I used the formula $I_z=1/12bh^3$ due to the fact that the cross section of the beam is rectangular. This value would be 846760.4167 mm^4 with the orientation used in the testing. The engineering stress was calculated by using the formula: $\sigma = \frac{M*c}{I_z}$, where M is the calculated moment, PL/8, and c is half the depth, 65/2 mm.
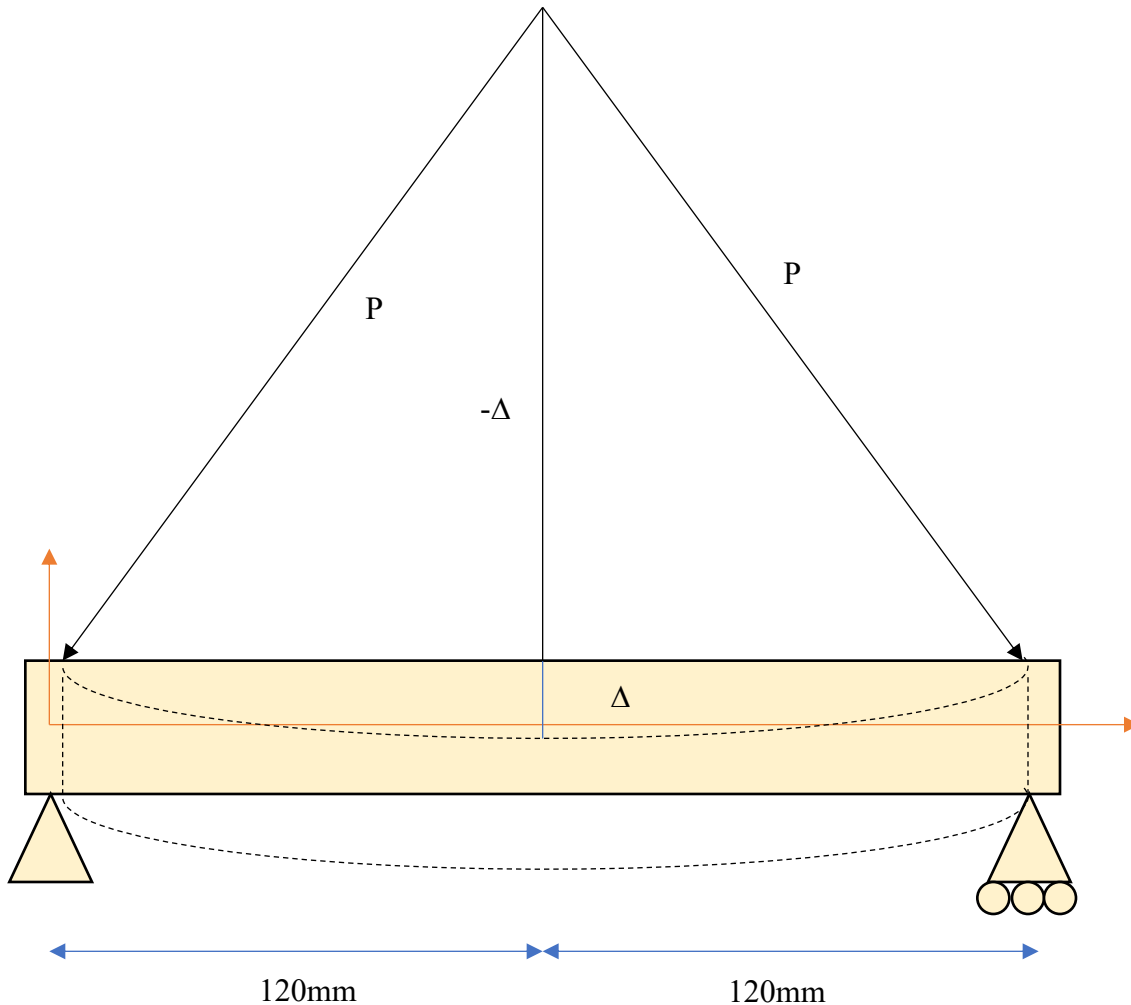
I calculated the engineering strain by using the formula: $\varepsilon = \frac{\Delta*d}{l^2}$, where d is the depth of the specimen (65 mm), Δ is the deflection that is given by the testing, and l is the loading span. The diagram above was used to derive the formula used to calculate the engineering strain.

5.3 Compressive Strength Test

For the compressive testing, a 4" by 8" sample was broken to get the compressive strength of the mix design.

5.3.1 Testing Procedure

The samples were measured for diameter and height. The first sample was broken without the extensometer to determine the stress at which the sample failed, so that I could avoid damaging the extensometer. The extensometer was attached using rubber bands, as shown in figure 5.5.

Figure 5.5: Testing Setup for Compressive Testing

I used this test to calculate the Elastic Modulus of the material. To calculate this, I used the following formula:

$$E = \frac{\sigma_1 - \sigma_2}{\varepsilon_1 - \varepsilon_2}$$

where σ and ε are taken from the linear portion of the stress-strain curve. For the graphs below, engineering strain was calculated by taking the change in position of the crosshead and dividing by the original height of the sample.

5.4 Brazil Disk Experiment

A Brazil Disk is a cylindrical sample with either no flaw or an induced flaw. The purpose of this method is to test the adhesion of the fibers in the sample.

5.4.1 Testing Procedure

The mix was cast into silicon molds. Three of the five molds had a tab in the middle of the sample that was 2 mm wide. After 24 hours, the samples were demolded and put into the curing room. The samples were tested using the standard format for split tensile tests. The samples with the induced flaw were tested with the flaw orientated vertically. Figure 5.6 shows the test setup I used. The wooden strips were used to prevent the material from crushing before the tensile load was reached.
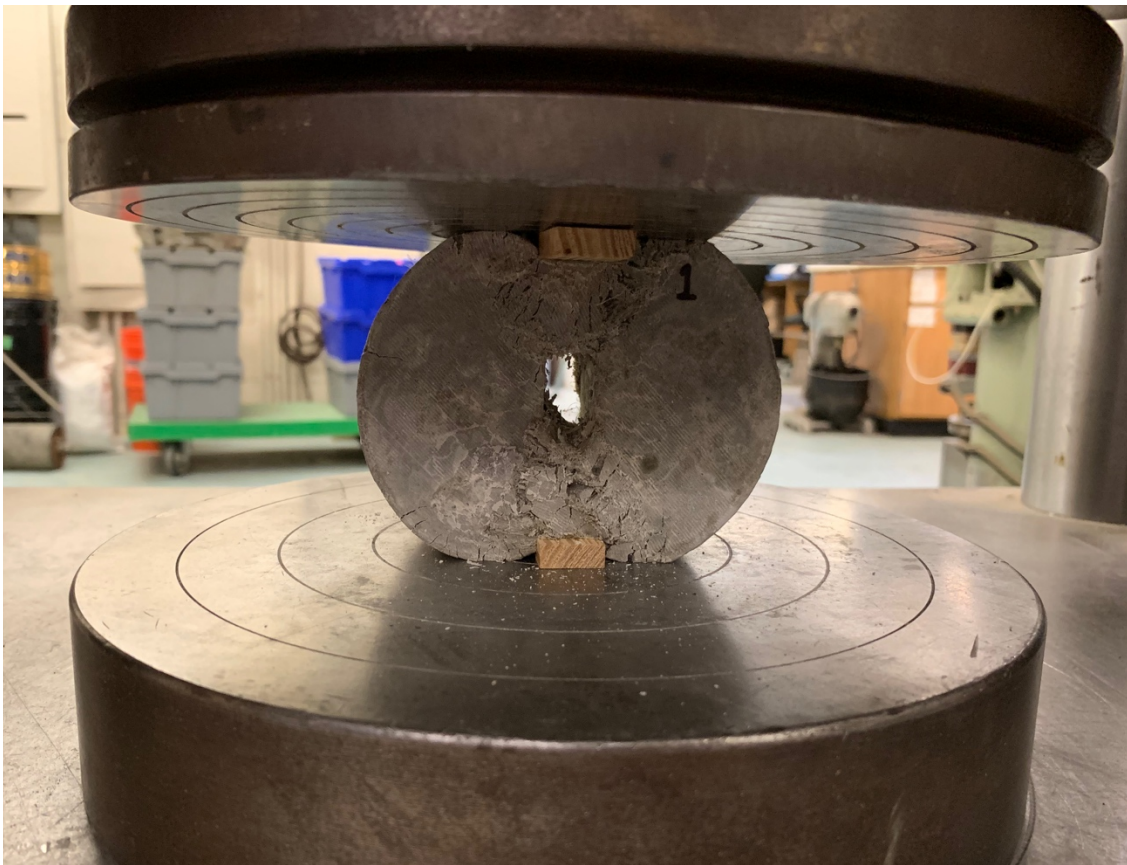

Figure 5.6: Testing of Sample 1

5.4.2 Calculations

The tensile strength of the material can be found using the following formula, which is given in the ASTM Standard: C496/C496M Standard Test Method for Splitting Tensile Strength of Cylindrical Concrete Specimens.

$$T = \frac{2P}{\pi l d}$$

Where:

T=tensile strength

P=maximum applied load

l=length

d=diameter

Chapter 6: Results & Discussion

In this chapter I discuss the new results achieved from improving the mixing process. For the results of Test Batch 1, see Section 4.3.

6.1 Four Point Bend Results

6.1.1 Test Batch 2

Test Batch 2 involved changing the mixing process. These samples were not mechanically vibrated. During the mixing process, the mix was more cohesive than in the first test batch, which used the original mixing process. When I was filling the molds for the original mixing process, the material in the bowl had a tendency to separate slightly from the water: some of the water would be on the surface of the mix and the cement, sodium bentonite, fibers and vermiculite would settle to the bottom of the bowl, so I had to mix by hand in between each scoop I put into the molds to make sure the water was evenly distributed. For test batch 2, the mix did not separate like the original mix did. The figure below shows the stress-strain curves for all the samples in test batch 2.
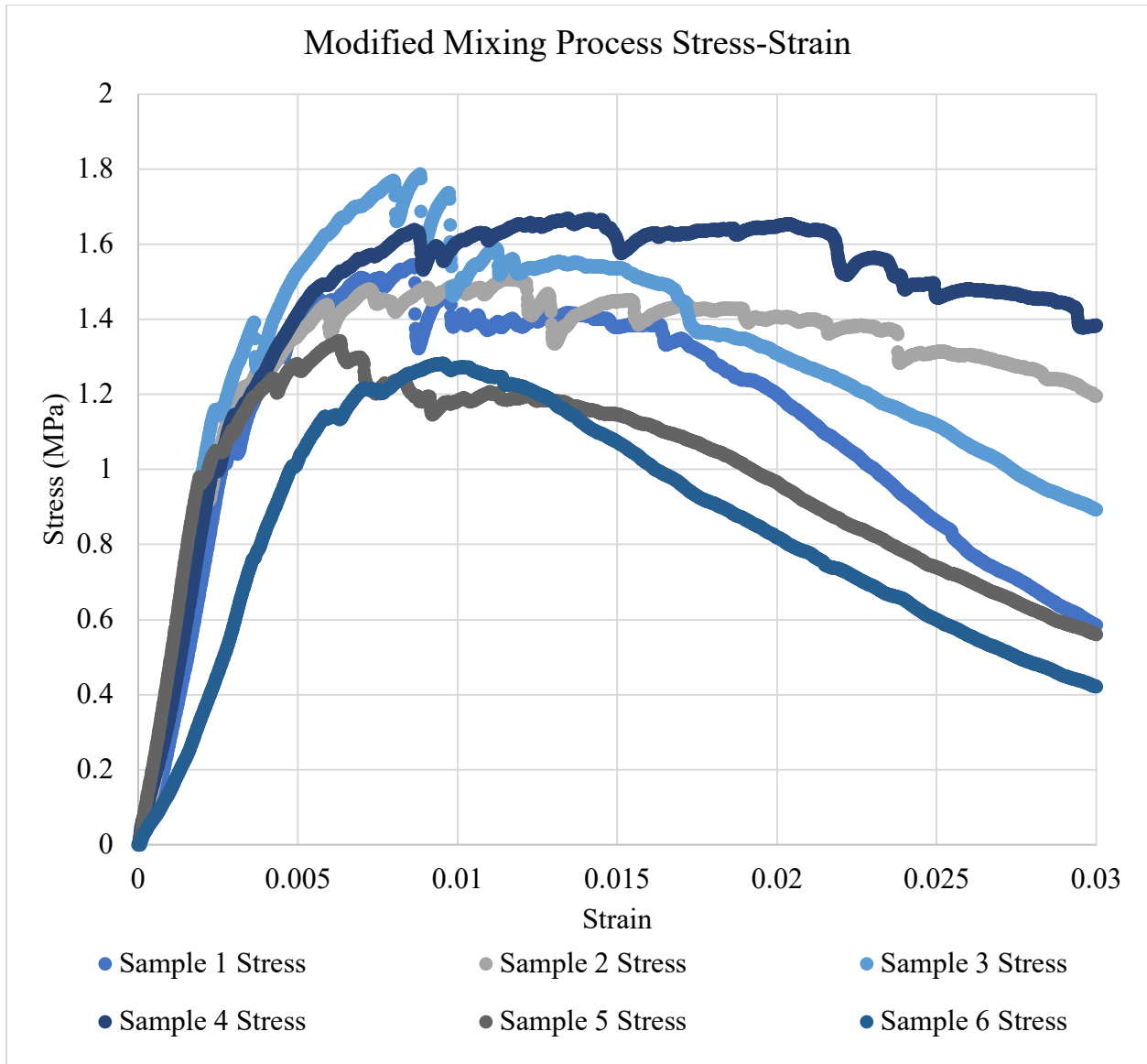
Figure 6.1: Test Batch 2 Stress-Strain Curve

As shown in Figure 6.1, the elastic region of the curves have similar slopes, and all the samples
except Sample 6 exhibit an extended period where the applied stress is relatively constant while
the engineering strain increases. Since the elastic region of the curves have similar slopes, the
Elastic Modulus of the batch is similar for the batch. All of the samples reached 1 MPa before
experiencing the first crack. The cracks that propagated through the samples never reached more
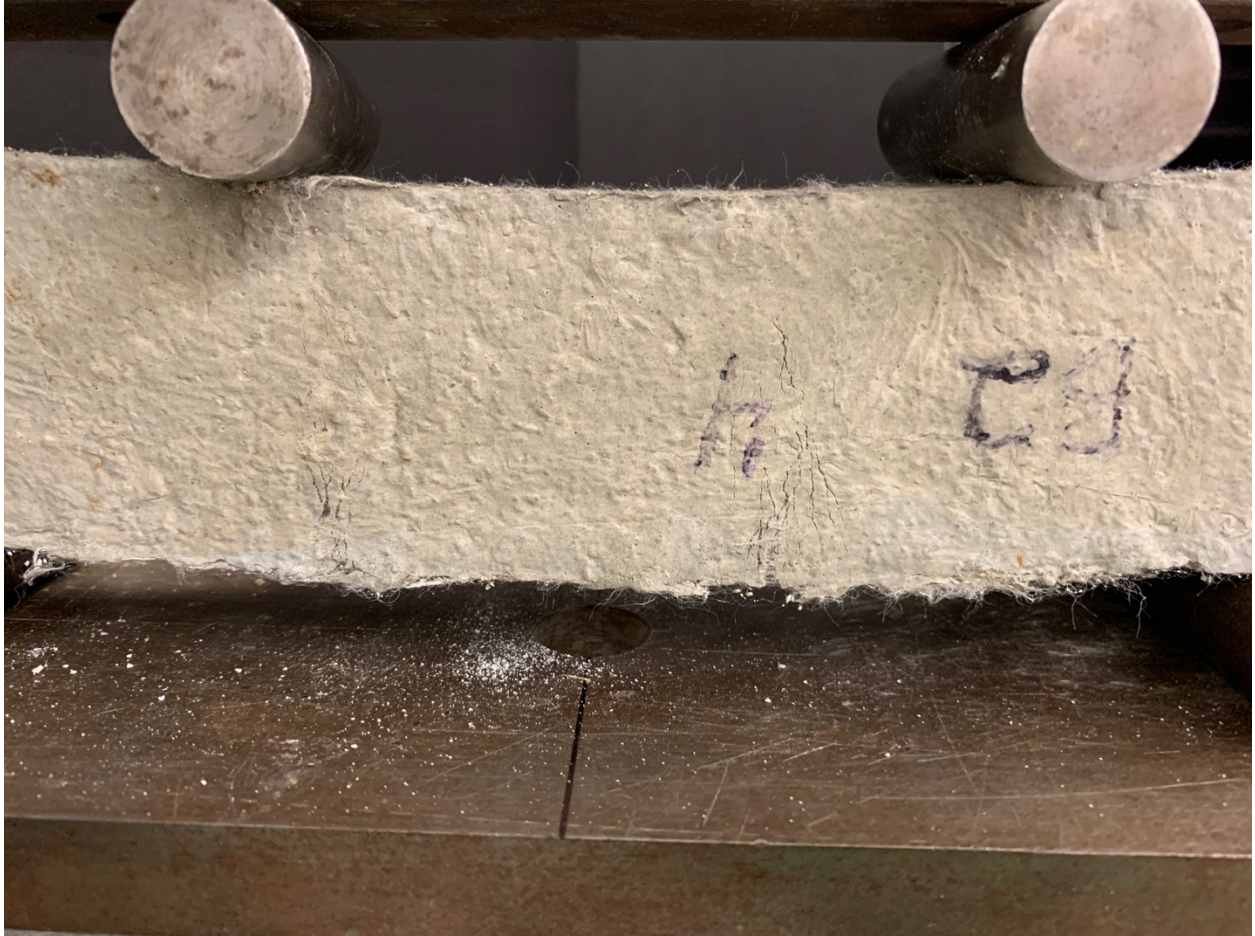than 75% of the way through the sample.

Figure 6.2: Multiple Cracking in Sample 4

In Figures 6.2 and 6.3, the cracking exhibited in these samples is similar to the cracking shown in Figure 4.5. There are multiple small cracks throughout the sample. The samples all had one large crack that propagated through about 75% of the sample. Once I looked at the unloaded sample, I noticed that all the large cracks started at points that had larger voids (about 2-4 mm) within the samples.
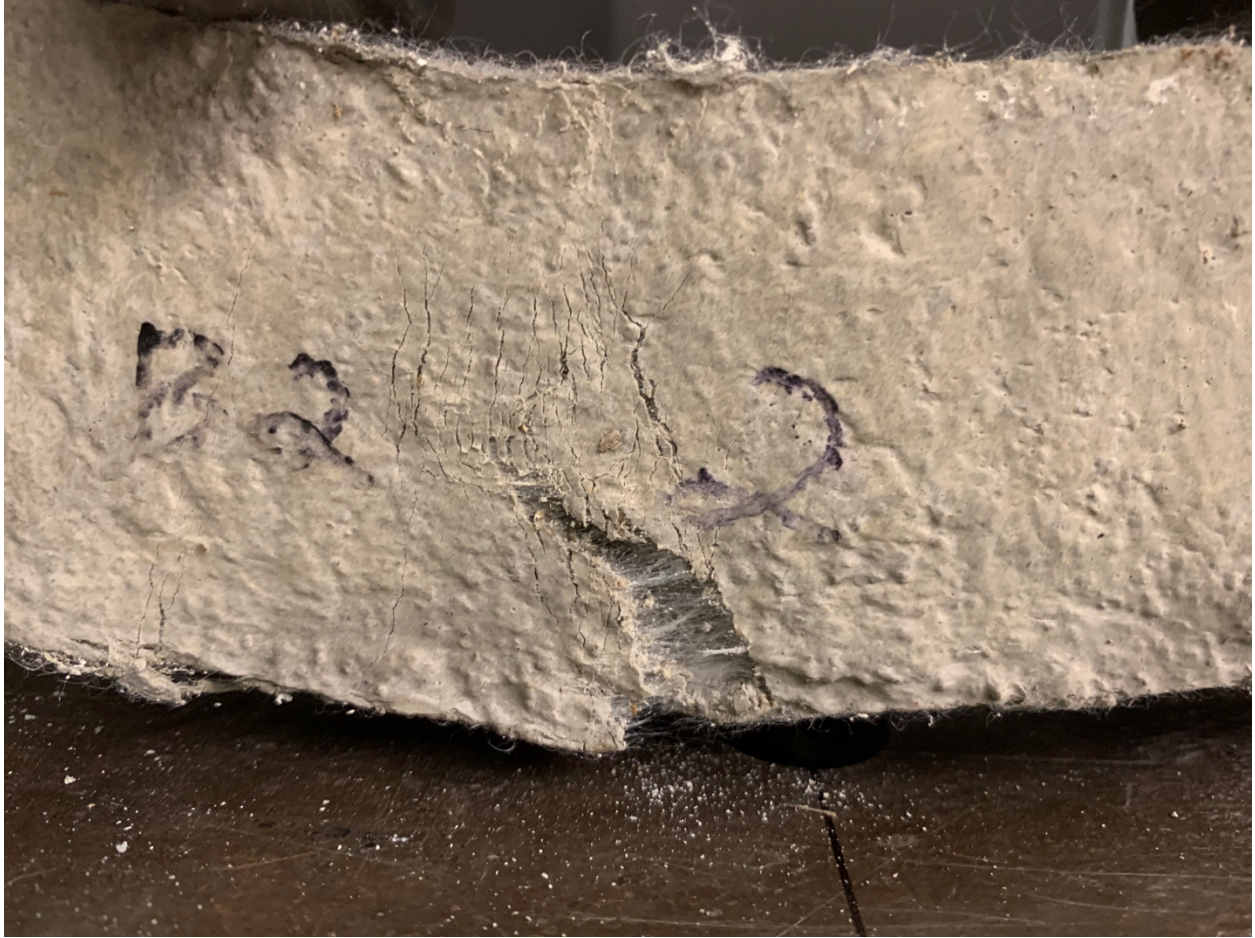
Figure 6.3: Cracking in Sample 2

6.1.2 Test Batch 3

Test Batch 3 used the modified mixing process and the samples were mechanically vibrated using a vibration table for about 4 minutes after being put into the molds. The figure below shows the stress-strain results for Test Batch 3.
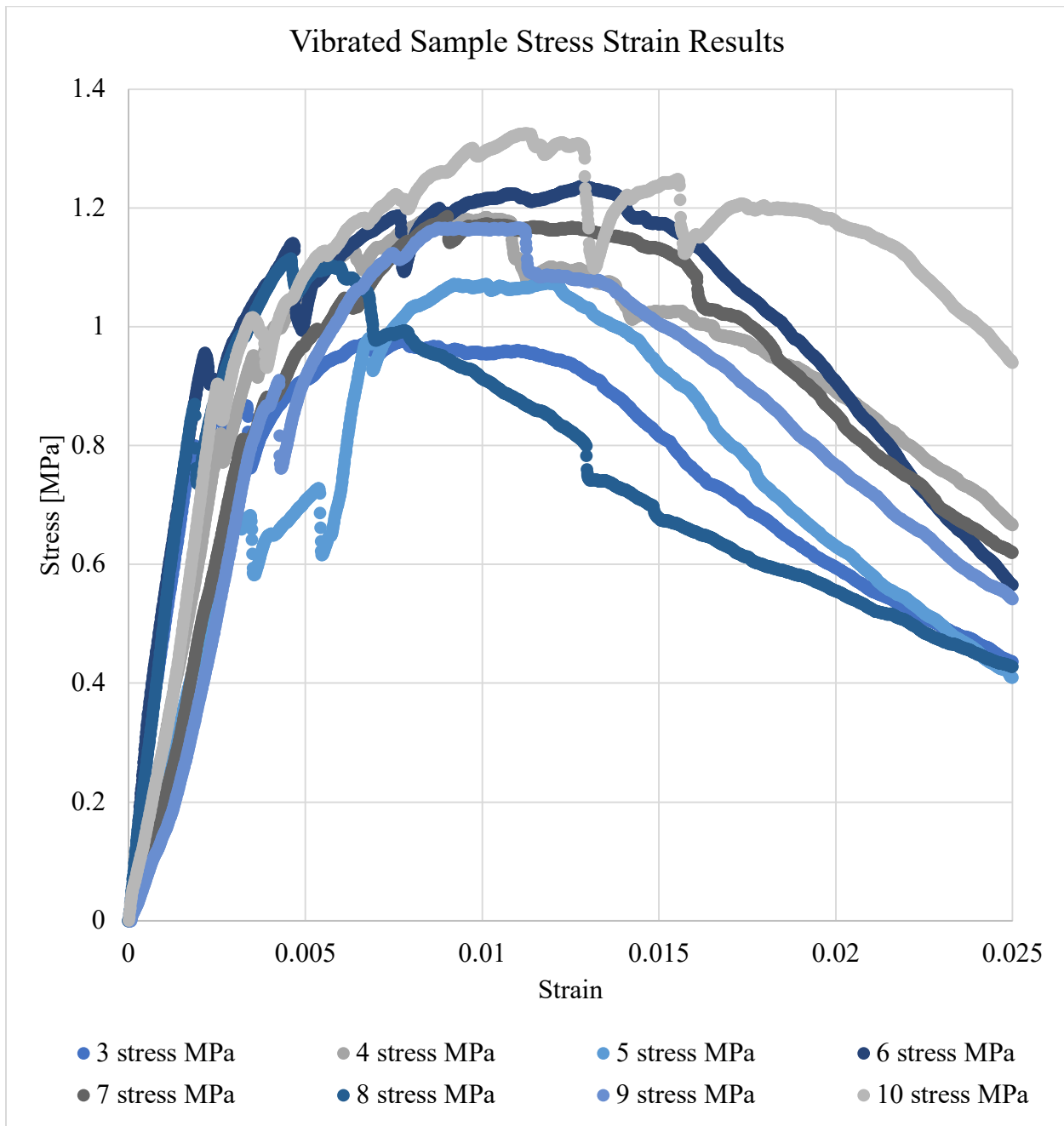
Figure 6.4: Stress-Strain Results of the Vibrated Samples

As shown in Figure 6.4, the results for the vibrated samples were not as consistent as Test Batch 2 and did not have the same elongated curve as Test Batch 2 either. Once the samples were unloaded, there were still voids within the sample. Vibration was used to try to eliminate some of the voids, but within the cracks there were more voids than the non-vibrated samples from Test Batch 2. Figure 6.5 shows the cracking patterns in some of the vibrated samples.

Samples 4 and 6 were the only samples that formed multiple cracks like the non-vibrated samples.
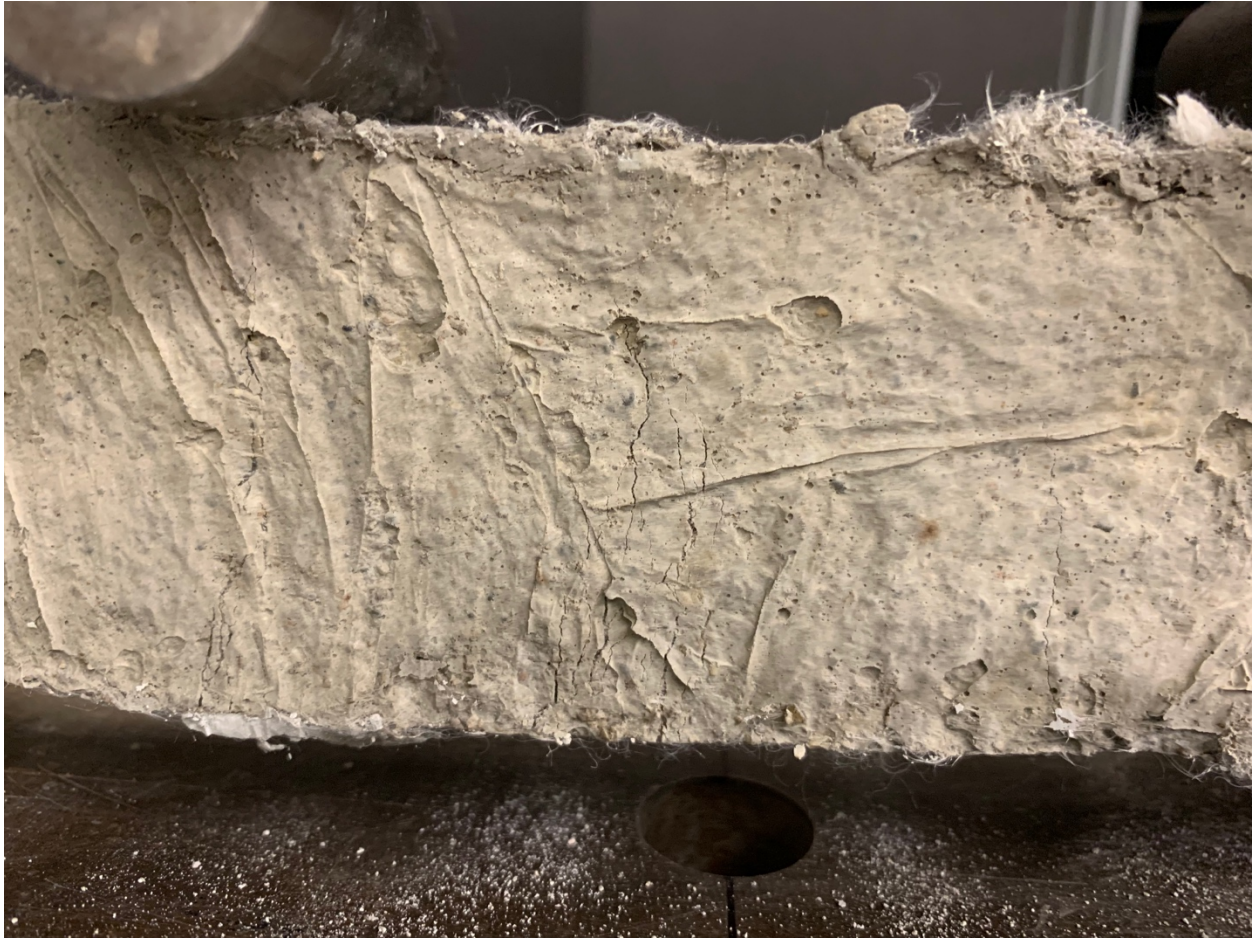

Figure 6.5: Vibrated Sample Cracking

6.2 Brazil Disk Results

6.2.1 Observations

Figures 6.6 to 6.10 show the samples the underwent the split tensile procedure. In each figure, there are shapes outlined in red. These shapes are outlining the cracking patterns. The common shape is the triangle at the top of each sample. This is the region where the sample underwent a tensile load. The triangle formed due to the ductility of the material. At the bottom of samples 2 and 3, there is the traditional cracking that is usually found in reinforced concretes. One observation from during the testing is that once the load was released from the samples, every single sample rebounded about ½". In each sample, near where the piece of wood was

placed is a small semi-circle of a compression zone, Figure 6.6 displays this more clearly, and is outlined in blue.
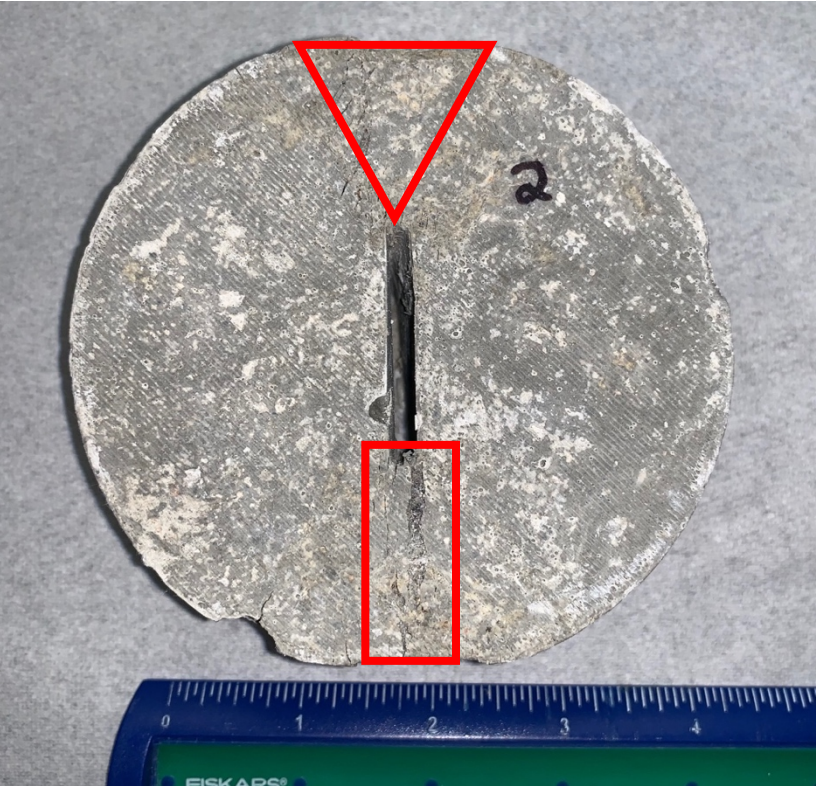

Figure 6.6: Brazil Disk Sample 1

Figure 6.7: Brazil Disk Sample 2

Figure 6.8: Brazil Disk Sample 3

Figure 6.9: Brazil Disk Sample 4

Figure 6.10: Brazil Disk Sample 5

6.2.2 Results

In Figure 6.11, all 5 of the curves have a similar peak load. Therefore, from these results the tensile strength of the material is notch insensitive. Samples 1, 2, and 3 all have the notch, and Samples 4 and 5 do not.
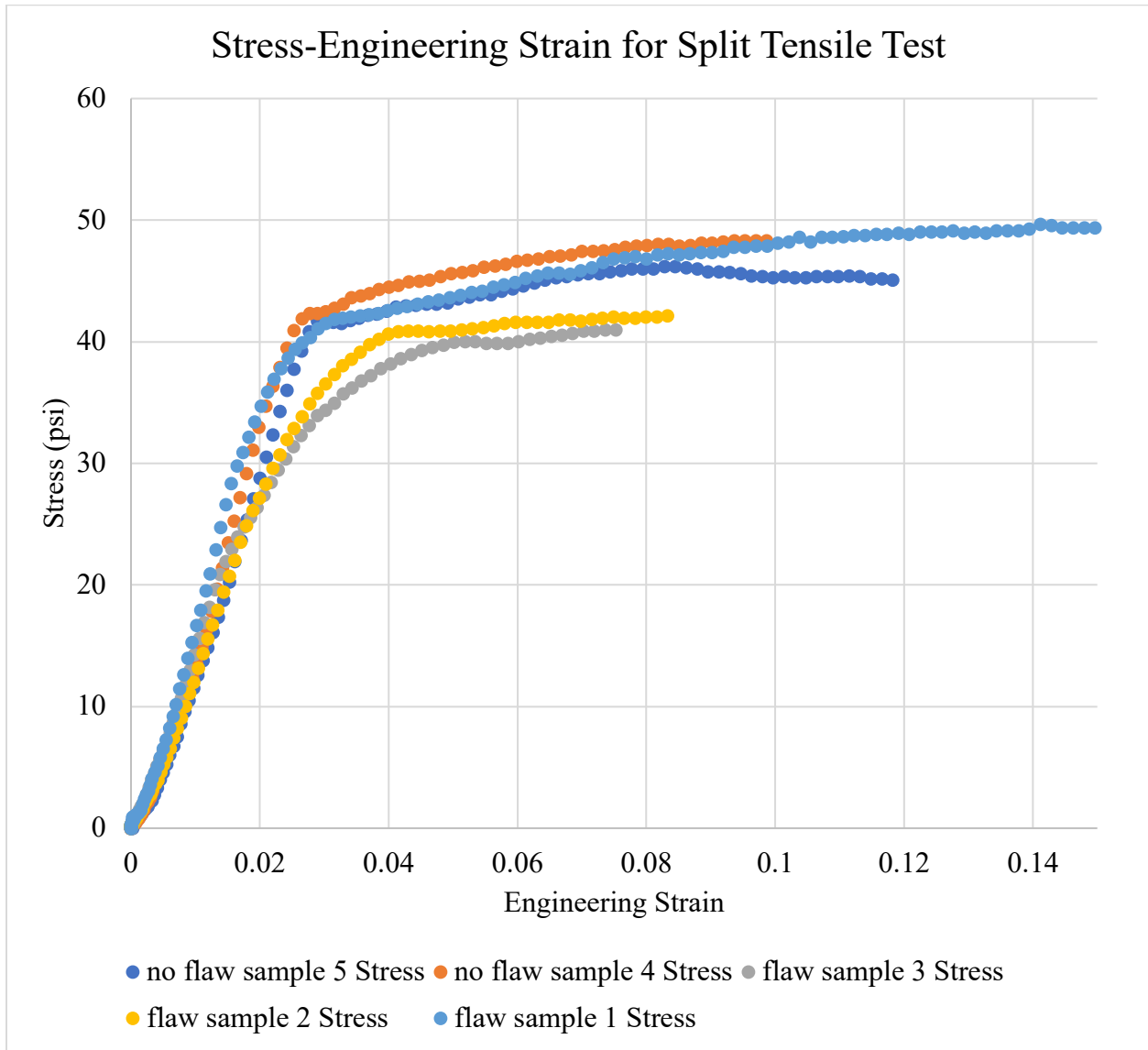
Figure 6.11: Brazil Disks and Split Tensile Disks

6.2.3 Calculations

For all the samples: the tensile strength of the material was calculated.

$$T_1 = \frac{2 * 478}{\pi * 3.899 * 1.849} = 42.21 \, psi$$

$$T_2 = \frac{2 * 473}{\pi * 3.921 * 1.866} = 41.156 \, psi$$

$$T_3 = \frac{2 * 470}{\pi * 3.929 * 1.943} = 39.194 \, psi$$

$$T_4 = \frac{2 * 489}{\pi * 3.918 * 1.878} = 42.309 \, psi$$

$$T_5 = \frac{2*500}{\pi * 3.919 * 1.949} = 41.674 \; psi$$

6.3 Compression Testing Results

6.3.1 Observations

During the testing, there were some things that I noted about the samples. In each test, the SFRM experienced the compression in discrete zones, instead of throughout the entire sample as a specimen of regular concrete would experience. About ½" to 1" at the top of the sample would experience the compression and crush, then once that zone failed, cracks would appear in the next ½" to 1" and so on (see Figure 6.17 for an annotated sample). The bottom of every sample was completely intact with no cracks or size change. The following figures show the samples that experienced the compression test. Figures 6.14-6.16 show the results of sample 1. Since sample 1 experienced the load the most, the patterns that start to appear in Samples 2 and 3 are more pronounced. In each sample, there is almost petal-like patterns at the top of the samples. The red circle in Figure 6.13 highlights one of these petal-like patterns. As Sample 1 shows, if the test continues further that "petal" would curl out more and if the sample was allowed to crush completely, the sample would open up like a flower. Another observation is about the final shape of the samples. Each sample has a flat portion at the top, then bulges out and then returns to another flat portion, which is the uncracked bottom. Out of the figures below, Figure 6.16 has the most obvious bulging pattern.

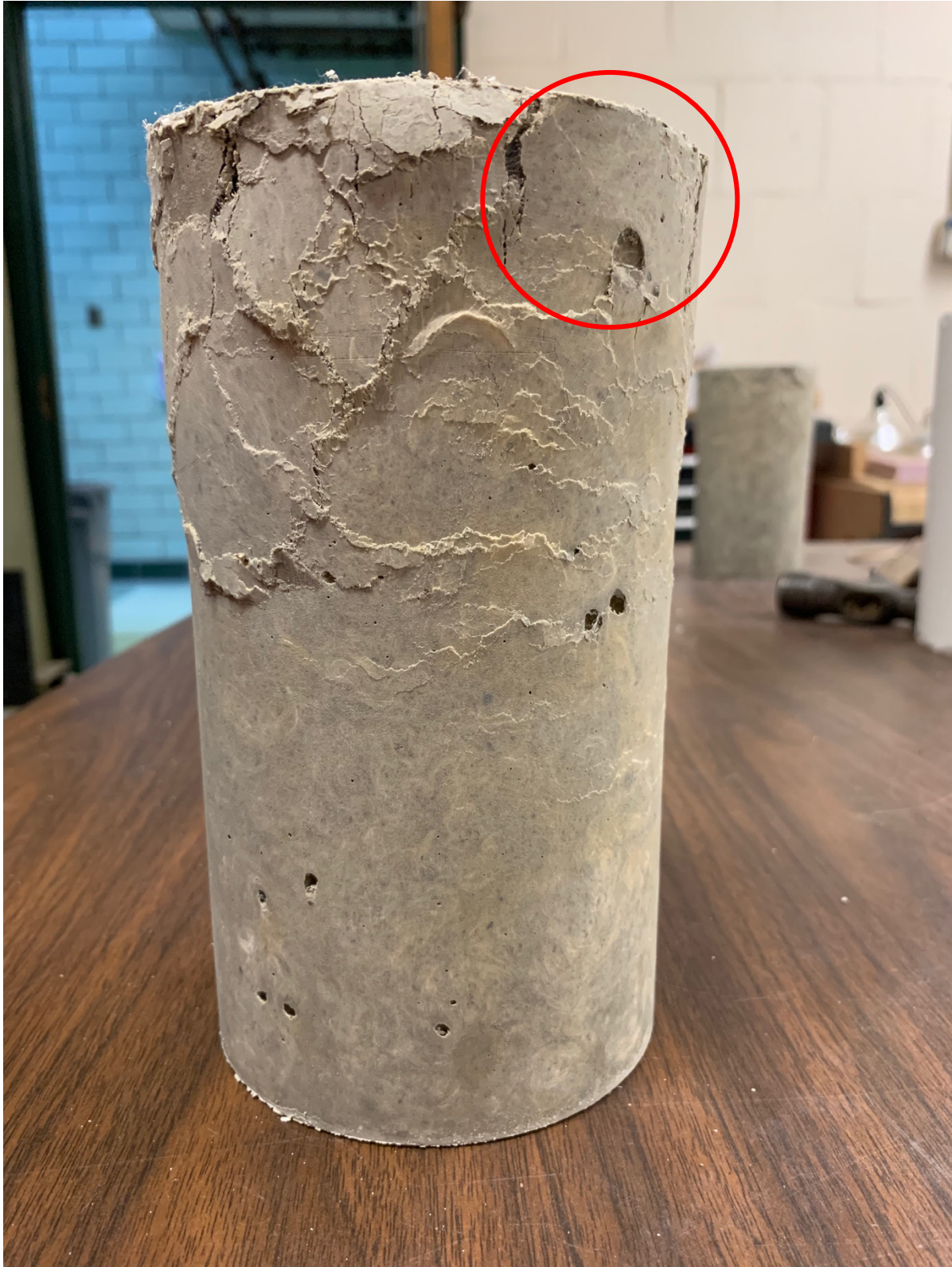Figure 6.12: Sample 2 Compression

Figure 6.13: Sample 2 Compression

Figure 6.14: Sample 1 Compression

Figure 6.15: Sample 1 Compression
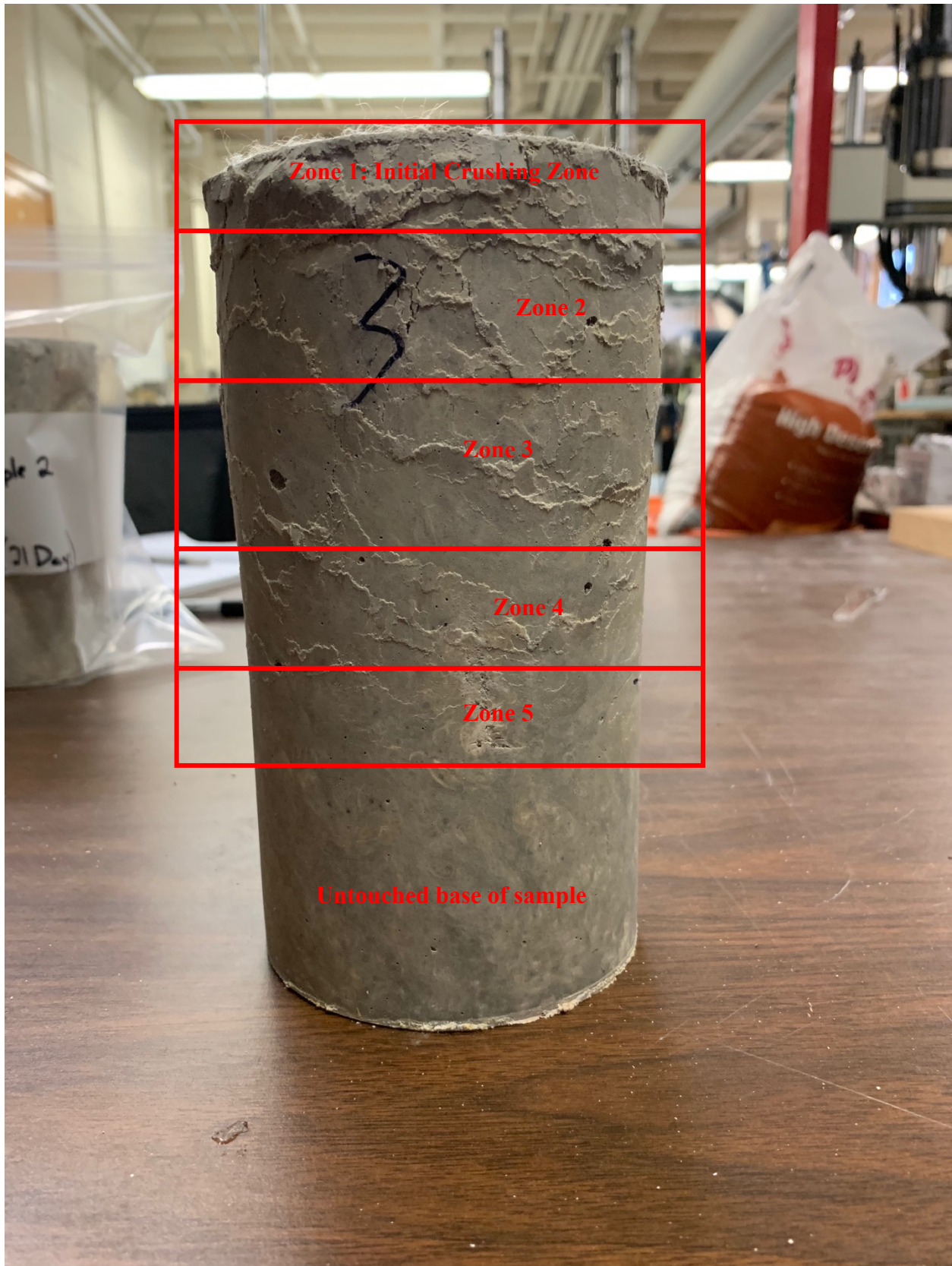
Figure 6.16: Sample 1 Compression

Figure 6.17: Sample 3 Compression (annotated)

Figure 6.18: Sample 3 Compression

6.3.2 Results and Calculations

The calculated modulus of elasticity for samples 2 and 3 was 7668.44 ksi and 7463.18 ksi, respectively. In Figure 6.19, the graph shows the stress over the engineering strain. The engineering strain was calculated by using the position of the loading cell and the original height of the sample. A second result that can be drawn from Figure 6.19 is the peak compressive stress the material can withstand. Sample 3 had a peak compressive stress of 260 psi. Sample 2 had a peak compressive stress of 250 psi, which gives an average compressive strength for the material at 21 days of 255 psi. The gap is from the removal of the extensometer.
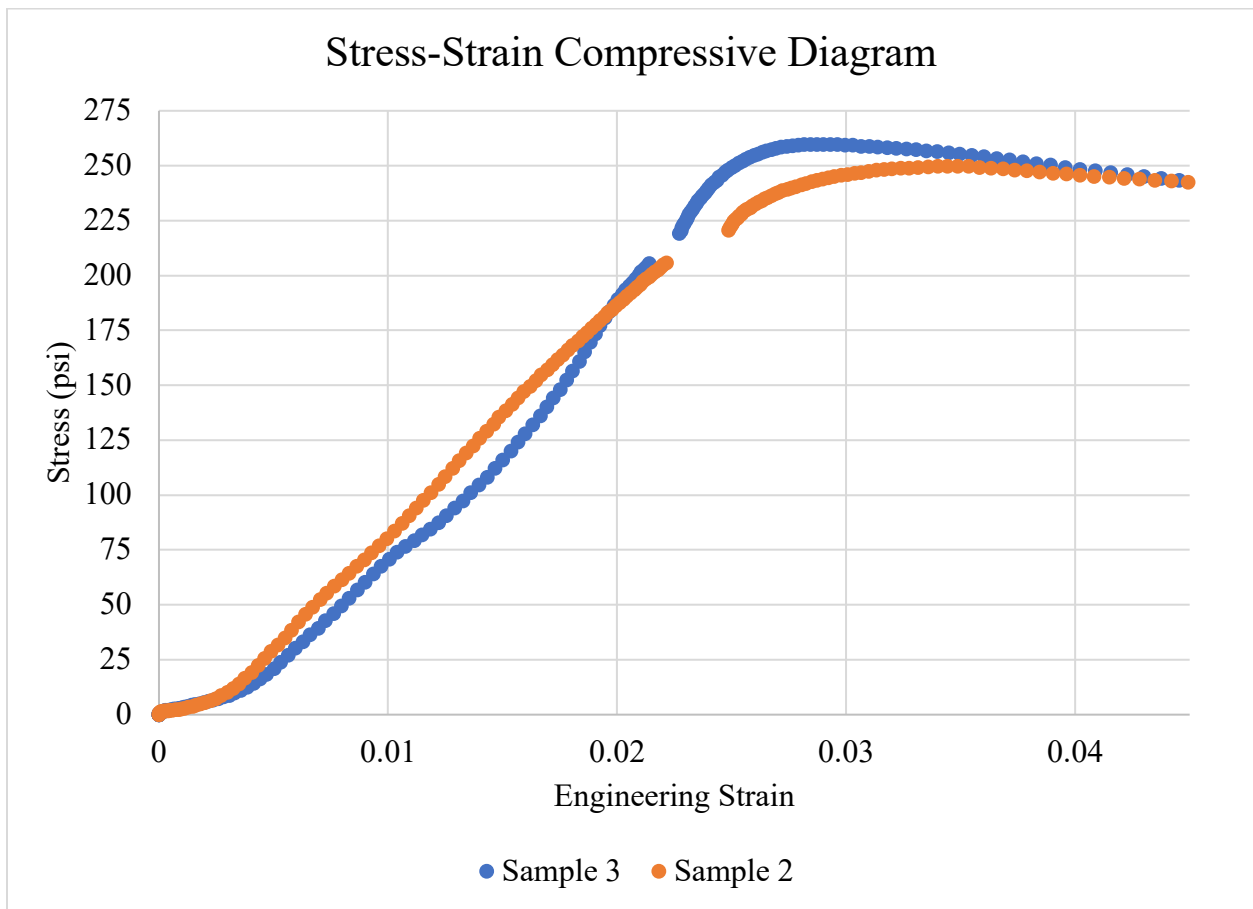

Figure 6.19: Stress over Engineering Strain

Figure 16.20 shows a common concrete with 3/8" aggregate and a water to cement ratio of 0.5 and the results of the SFRM. The graph shows the vast difference between the way normal concrete breaks and the SFRM in this study breaks. Besides the zoned compression that the SFRM experienced, once the load is released from the sample, there was a rebound of about ½" in every sample tested in compression. The regular concrete sample crack with two cones. When the SFRM started to crush, the bottom of the specimen was completely intact and had no

deformation or cracking. The ductility the SFRM has compared to regular concrete is important to note as current SFRMs can be very brittle. The concrete only reached an engineering strain of about 1%, while the SFRM reached a strain of about 6%. The behavior of the SFRM is closer to the behavior of a steel specimen or a more ductile section rather than a traditional concrete.
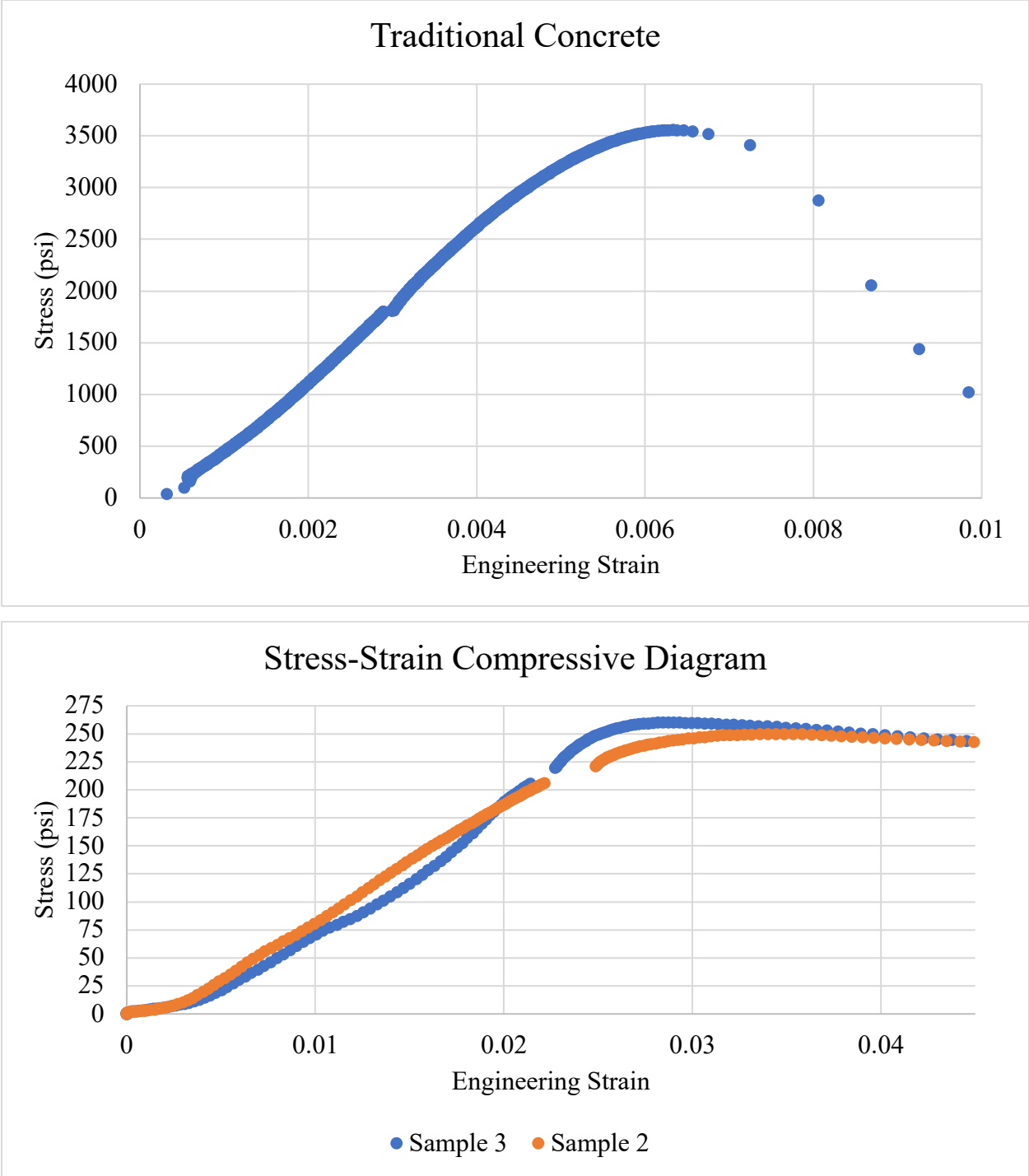

Figure 6.20: Comparison of the SFRM to Concrete with Regular Aggregate

6.4 Discussion of Results

In Chapter 4, the replication of previous results was covered. In these tests, the results of the testing varied and was not consistent. Figure 4.9 shows the stress-strain curve of the samples from exactly replicating the mixing process. Unlike the new mixing process, the samples did not have multiple cracks and did not have the elongated flat portion of the curve. Table 6.1 shows a summary of the new peak stresses compared to the original mixing process on the SFRM. Table 6.2 compares the new mixing process results to previous work done on the SFRM Project.

Table 6.1: Comparison of Results from Replicated Mixing to New Mixing Process				
Test Method	New Mixing Process		Original Mixing Process	
	Average Peak Stress [psi]	Engineering Strain [in/in]	Average Peak Stress [psi]	Engineering Strain [in/in]
4-Point Bend	203 (1.4 MPa)	0.03	162 (1.12 MPa)	0.025
Compression	260	0.04	N/A	N/A
Split Tensile	40	>0.06	N/A	N/A

Table 6.2: Comparison of Previous Work to New Mixing Process		
Result	Average Peak Stress [psi]	Engineering Strain [in/in]
Previous Work	130 (0.9 MPa)	0.045
New Mixing Process	203 (1.4 MPa)	0.03

From the compression stress-strain curves and the split tensile stress-strain curves and cracking patterns, the peak stress of the samples by the new mix has significantly increase. Figure 6.20 has a comparison of the SFRM to regular, unreinforced concrete. The enhancement in the ductility of the samples is clearly demonstrated, as the regular concrete peaked, then the stress immediately dropped and the strains the sample experienced is less than 0.01, while the proposed composite continued to level off at a stress around 250 psi and maintained that stress level throughout the test to a strain value greater than 0.06, which was when the test was stopped since the stress had not dropped more than 20%.

Chapter 7: Conclusion

There are some conclusions that can be drawn from the results presented in Chapter 6. From the 4-point bend test, the first crack did not appear in the samples until after 1 MPa (145 psi), the cracks did not propagate through the entire material and the specimens experienced almost ductile like bending due to the crack patterns present. Ductility and limited crack propagation in bending is important for a SFRM because beams often experience bending moments and as SFRMs are applied to beams, they will also experience bending. The limited crack propagation is important, as the samples did not break, so there would be no exposed steel faces on the beam the SFRM is coating.

From the compression tests, the samples crushed in zones and left one face entirely intact. Since there was 1 face intact, even if the outside or inside of the SFRM fails due to the compression in the SFRM, the opposite face will still be protecting the steel, even though the other face has failed.

The split tensile tests and Brazil Disk tests demonstrate that regardless of the presence of a flaw, the material will crack at the same load. This is important for an SFRM to have because if there is an application error, then the SFRM will not start cracking before a perfectly applied section. Another conclusion that can be drawn from the split tensile tests is from the unusual behavior the samples exhibited. Instead of reacting like pure concrete, the samples experienced tensile zones and had triangular sections of cracking that show the ductility of the material. The rebound that all the split tensile samples experienced, and the compressive samples experienced also show the ductility of the material.

There are some recommendations for continuing the project or for improvements to the project. One recommendation for the next iteration of the project would be to conduct thermal testing and to test the adhesion of the proposed material to steel. Another recommendation I have would be to try different fiber sizes. If a smaller fiber is used, it might help to make the samples more consistent and will prevent the cracks from opening up as wide. A second recommendation relating to the fibers, would be to try different fiber types. A third recommendation would be to continue testing brazil disks and split tensile tests to see if all the samples are as consistent as the five that I tested.

Chapter 8: References

Bentur, A. & Mindess S., Fiber Reinforced Cementitious Composites, Taylor & Francis, 2007.

Brannigan, F. L. (1982). *Building Construction for the Fire Service.* NFPA (2nd edition).

Braxtan, N. L. and S. P. Pessiki. "Postearthquake Fire Performance of Sprayed Fire-Resistive Material on Steel Moment Frames," Journal of Structural Engineering ASCE, 137(9), 946-953, 2011.

Bunsell, A. R. (2009). *Handbook of tensile properties of textile and technical fibres*. Oxford: Woodhead.

Grolms, Martin. (2015), Bentonite in Drilling Mud, https://www.advancedsciencenews.com/bentonite-drilling-mud/

Kourkoulis, S. K. and Markides, C. F. "Fracture Toughness Determined by the Centrally Cracked Brazilian-Disc Test: Some Critical Issues in the Light of an Alternative Analytic Solution," *Materials Performance and Characterization*, Vol. 3, No. 3, 2014, pp. 45-86, https://doi.org/10.1520/MPC20130056. ISSN 2165-3992

Papp J.E. (1996) Sodium Bentonite as a Borehole Sealant. In: Fuenkajorn K., Daemen J.J.K. (eds) Sealing of Boreholes and Underground Excavations in Rock. Springer, Dordrecht

Pierre-Claude Aïtcin, Robert J Flatt, *Science and Technology of Concrete Admixtures*, 3 - Portland cement, Woodhead Publishing, 2016, Pages 27-51, https://doi.org/10.1016/B978-0-08-100693-1.00003-5. (http://www.sciencedirect.com/science/article/pii/B9780081006931000035)

Pierre-Claude Aïtcin, Robert J Flatt, *Science and Technology of Concrete Admixtures*, 4 - Supplementary cementitious materials and blended cements, Woodhead Publishing, 2016, Pages 53-73, https://doi.org/10.1016/B978-0-08-100693-1.00004-7. (http://www.sciencedirect.com/science/article/pii/B9780081006931000047)

Ruddy, J. L., Marlo, J. P., Ioannides, S. A., & Alfawakhiri, F. (2003). *Fire Resistance of Steel Structural Framing*, American Institute of Steel Construction.

Shalchy, F., & Rahbar, N. (2015). Nanostructural Characteristics and Interfacial Properties of Polymer Fibers in Cement Matrix. *ACS Applied Materials & Interfaces*, 7(31), 17278-17286.

Wang, Y., Burgess, I., Wald, F., Gillie, M. (2013). Performance-Based Fire Engineering of Structures. London: CRC Press, https://doi.org/10.1201/b12076

Zhang, Q., and Li, V. C. (2015). "Development of durable spray-applied fire-resistive Engineered Cementitious Composites (SFR-ECC)," Cement & Concrete Composites, no. 60, pp. 10-16.

Zhang, Q., and Li, V. C. (2014) "Adhesive bonding of fire-resistive engineered cementitious composites (ECC) to steel," Construction and Building Materials, no. 64, pp. 431-439.